GELATIN NANOPARTICLE LOADED POLYCAPROLACTONE-NANOHYDROXYAPATITE FUNCTIONALLY GRADED SCAFFOLDS

Özlem Araç

Submitted to the Graduate School of Engineering and Natural Sciences

In partial fulfilment of the requirements for the degree of

Master of Science

Sabanci University

December 2023

GELATIN NANOPARTICLE LOADED POLYCAPROLACTONE-
NANOHYDROXYAPATITE FUNCTIONALLY GRADED SCAFFOLDS

GELATIN NANOPARTICLE LOADED POLYCAPROLACTONE-NANOHYDROXYAPATITE FUNCTIONALLY GRADED SCAFFOLDS

Özlem Araç

Master of Science Thesis, 2023

Supervisor: Assoc. Prof. Güllü Kızıltaş Şendur

Keywords: Functionally graded scaffold, 3D printing, gelatin nanoparticle, BMP-2 release, poly(caprolactone), hydroxyapatite, bone scaffold

Abstract

Bone fractures represent a common medical challenge, necessitating innovative approaches for effective bone tissue regeneration. This thesis explores the potential of controlled bone morphogenetic protein-2 (BMP-2) release from functionally graded (FG) vs. uniform scaffolds made of Polycaprolactone (PCL) and Nanohydroxyapatite (HA) incorporating gelatin nanoparticles. The scaffolds were fabricated using a combination of the earlier proposed Non-Solvent-Induced Phase Separation (NIPS) method and 3D printing and therefore display multi-scale porosity and spatially varying macropores mimicking natural bone tissue. Gelatin nanoparticles (GNP) were created through a two-step desolvation method, and BMP-2 was encapsulated into these nanoparticles using a diffusion method. The incorporation of BMP-2 encapsulated gelatin nanoparticles into PCL-HA scaffolds of uniform and FGSs was achieved through adsorption. Of particular significance, this study investigates the effect of morphology and BMP-2-gelatin nanoparticle loading on biological and release performance of uniform and functionally graded scaffolds (FGSs). The macro porosity gradient and internal micro-porosity was analysed using micro-computed tomography (micro-CT). Tensile tests using universal tensile machine (UTM) were conducted on both uniform and FGSs to assess their mechanical strength. The variation in macro-scale porosity gradient of multi-scale porous scaffolds and its influence on in-vitro performance and release mechanism constitute the primary focus of this research and were analysed using phalloidin and DAPI staining and alkaline phosphatase activity (ALP) assays as well as enzyme linked immunosorbent assay (ELISA) and confocal microscopy. Scanning electron microscopy (SEM) was conducted to visualize the GNP structure and microstructure of scaffolds. The results underscore the viability of fabricating scaffolds via NIPS-based 3D printing and loading them via BMP-2 GNP demonstrating the potential for sustained release of BMP-2 encapsulated gelatin nanoparticles in 3D scaffolds with gradient and multi-scale porosity. The findings contribute to the understanding of how porosity gradients influence the in-vitro performance of these scaffolds, providing valuable insights for the design and optimization of tissue engineering constructs.

JELATİN NANOPARÇACIK YÜKLÜ POLİKAPROLAKTON-
NANOHİDROKSİAPATİT FONKSİYONEL OLARAK KADEMELİ İSKELELER

Özlem Araç

Yüksek Lisans Tezi, 2023

Tez Danışmanı: Doç. Dr. Güllü Kızıltaş Şendur

Özet

Kemik kırıkları yaygın bir tıbbi sorunu temsil eder ve etkili kemik doku yenilenmesi için yenilikçi yaklaşımlara ihtiyaç duyar. Bu tez, Polikaprolakton (PCL) ve Nanohidroksiapatit (HA) içeren jelatin nanopartiküller (GNP) kullanan düzenli ve fonksiyonel dereceli iskelelerin (FGS) kontrol edilen kemik morfogenetik protein-2 (BMP-2) salınım potansiyelini araştırmaktadır. İskeleler, daha önce önerilen Non-Solvent-Induced Phase Separation (NIPS) yöntemi ve 3D baskı kombinasyonu kullanılarak üretildiğinden, doğal kemik dokusunu taklit eden çok ölçekli porozite ve fonksiyonel olarak değişen makroporları sergiler. Jelatin nanopartikülleri, iki aşamalı desolvasyon yöntemi kullanılarak üretildi ve BMP-2'nin bu nanopartiküller içine kapsüllenmesi difüzyon yöntemiyle yapıldı. BMP-2 kapsüllenmiş jelatin nanopartiküllerin, uniform ve FGS PCL-HA iskelelerine adsorpsiyon yoluyla entegrasyonu sağlandı. Bu çalışma özellikle morfolojinin ve BMP-2-jelatin GNP yüklemenin düzenli ve fonksiyonel dereceli iskelelerin biyolojik ve salınım performansı üzerindeki etkisini araştırmaktadır. İskelelerin makro porozite gradyanı ve içsel mikro-porozitenin çok ölçekli poroz yapısı mikro-CT kullanılarak analiz edildi. In-vitro performans ve salınım mekanizması üzerindeki etkisi araştırıldı. Düzenli ve fonksiyonel dereceli iskelelerin mekanik dayanıklılığını değerlendirmek için her iki iskele üzerinde çekme testleri universal çekme cihazı (UTM) ile gerçekleştirildi. Çok ölçekli poroz iskelelerin makro ölçekli porozite gradyanındaki değişim ve bunun in-vitro performans ve salınım mekanizması üzerindeki etkisi, phalloidin ve DAPI boyama ve ALP deneyleri, ELISA testleri ve konfokal mikroskopi kullanılarak analiz edildi. NP yapısını ve iskelelerin mikroyapısını görselleştirmek için SEM yapıldı. Sonuçlar, NIPS tabanlı 3D baskı kullanarak iskelelerin üretilebilirliğini ve BMP-2 GNP yükleme ile onları yükleme potansiyelini vurgular, böylece gradient ve çok ölçekli poroziteye sahip 3D iskelelerde BMP-2 içeren jelatin nanopartiküllerin sürdürülebilir salınım potansiyelini gösterir. Bulgular, porozite gradyanlarının bu iskelelerin in-vitro performansını nasıl etkilediğine dair anlayışa katkıda bulunur, doku mühendisliği yapılarının tasarımı ve optimizasyonu için değerli görüşler sunar.

To my dearest family…

TABLE OF CONTENTS

LIST OF FIGURES

LIST OF TABLES

List of Abbreviations

3D	Three dimensional
ALP	Alkaline Phosphatase
BMP-2	Bone morphogenetic protein
BSA	Bovine serum albumin
CAD	Computer aided design
DAPI	4′,6-Diamidino-2-Phenylindole
DPBS	Dulbecco's phosphate-buffered saline
ECM	Extracellular matrix
ELISA	Enzyme-linked immunosorbent assay
FBS	Fetal bovine serum
FGS	Functionally graded structure
GA	Glutaraldehyde
GNP	Gelatin nanoparticles
HA	Hydroxyapatite
MC3T3-E1	Mus musculus calvaria
Micro-CT	Micro Computational Tomography
M-PER	Mammalian Protein Extraction Reagent
MTS	3-(4,5-dimethylthiazol-2-yl)-5-(3-carboxymethoxyphenyl)-2-(4-sulfophenyl)-2H-tetrazolium
NIPS	Non-solvent Induced Phase Separation
PCL	Polycaprolactone
PLA	Polylactic acid
PLGA	Poly (lactic-*co*-glycolic acid)
SEM	Scanning Electron Microscopy
THF	Tetrahydrofuran
UTM	Universal Testing Machine
μ, um	Microns

Acknowledgement

I would like to extend my sincere appreciation to my supervisor, Assoc. Prof. Güllü Kızıltaş Şendur, for her unwavering guidance throughout my master's thesis. I would also like to thank Assist. Prof. Sibel Çetinel for her collaboration as a part of this thesis. I would also like to thank my jury members, Assist. Prof Sibel Çetinel and Prof. Ayşe Elif Erson Bensan for their valuable feedback.

I would like to express my gratitude to my group members, Mervenaz Şahin, Işıl Demirkan, and Sezen Öztürk. They consistently provided assistance and support throughout my studies.

I would also like to extend my appreciation to all my friends, Eda Şutova, Ebru Demir, Sevilay Burcu Şahin, and Asena Gülenay Tatar for their valuable help and moral support throughout this thesis.

I would like to express my special thanks to Görkem Ferah for his unwavering support, patience, and encouragement.

Last but certainly not least, I extend my most sincere gratitude to my family. Your constant presence, love, support, understanding, and care have meant the world to me.

Chapter 1

Introduction

1. Motivation

Infections, trauma, or congenital physical issues commonly give rise to bone defects. When these defects exceed critical-size limits, the need for bone transplants arises, which may include autografts, allografts, or synthetic biomaterials. Given the high cost associated with bone transplants and the demand for cost-effective alternatives, tissue scaffolds emerge as an attractive option.

The desired properties of scaffolds encompass biocompatibility, biodegradability, mechanical properties mimicking those of natural bone, appropriate porosity for nutrient diffusion and cell infiltration, a three-dimensional structure resembling the extracellular matrix, and surface chemistry conducive to cell adhesion. Furthermore, scaffolds should exhibit osteoconductive properties, a controlled degradation rate aligned with tissue regeneration, incorporation of bioactive components to enhance regenerative potential, and adherence to sterility and safety standards (Pina et al., 2019). Complementing these scaffold characteristics, the success of osteoinduction also depends on the presence of undifferentiated stem cells and bioactive factors like bone morphogenetic proteins (BMPs). However, these bioactive factors present challenges related to stability, half-life, and concentration, which can be addressed through the development of a slow-release system using scaffolds to control the release sequence and rate of bioactive factors (Vesvoranan et al., 2022). The loading of bioactive agents onto scaffolds can be accomplished through three primary methods: non-covalent bonding, covalent bonding, and encapsulation into micro or nanoparticles (Pei et al., 2023).

Gelatin nanoparticles (GNP), due to their biocompatibility and versatility, are often employed for bioactive agent delivery. These nanoparticles can encapsulate various therapeutic agents, facilitating controlled release and targeted delivery to specific tissue

sites. The choice of a two-step desolvation process offers distinct advantages in the fabrication of gelatin nanoparticles. This method allows for precise control over the particle size, morphology, and drug encapsulation efficiency (Yasmin et al., 2017). *Therefore, in this thesis we produce GNPs using a two-step desolvation method into Functionally Graded Scaffolds (FGS) and uniform scaffolds made of Polycaprolactone (PCL) and nano-hydroxyapatite (HA) to study their effect on their biological response and release performance.*

Throughout the years, various fabrication techniques have been employed to obtain scaffolds with these desired properties. One commonly utilized method is electrospinning, which involves the electrostatic spinning of polymer solutions into nanofibrous matrices that possess a high surface area and porosity. Freeze-drying, also known as lyophilization, is another technique utilized to produce porous scaffolds. This process involves freezing the scaffold and removing the water content, thereby preserving its porous structure. Additionally, salt-leaching is a technique that involves the use of salt particles as sacrificial templates. These salt particles dissolve, leaving behind a porous scaffold structure (Maia et al., 2022a). Another widely used technique is 3D printing, which allows for the layer-by-layer deposition of biomaterials, resulting in the creation of complex scaffold structures with precise control over their geometry (Koons et al., 2020a). Within these manufacturing methods, a notable technique is the integration of non-solvent induced phase separation (NIPS) with 3D printing.

Explorations into 3D printing through the NIPS method have demonstrated the production of consistent 3D structures featuring micro and macro pores (J. W. Kim et al., 2017a). However, it is crucial to highlight that existing investigations have not yet delved into the effects of non-uniform macro-porosity, or functionally graded scaffold morphologies, in particular the integration of BMP-2 loaded gelatin nanoparticles into FGS remains unexplored which is the main motivation of this thesis.

2. Objective

The primary objective of this research is to address the knowledge gap in existing literature related to the performance analysis of scaffolds mimicking the natural bone tissue, namely, FGSs in comparison to their uniform counterparts both with inherent multi-scale porosity when loaded with BMP-2 encapsulated GNPs. The study intends to

utilize NIPS-based 3D printing technology in order to produce FGSs while examining the impact and release kinetics of BMP-2 loaded GNPs.

Towards these objectives, the scaffolds analysed in this thesis were fabricated using a combination of the earlier proposed Non-Solvent-Induced Phase Separation (NIPS) method and 3D printing and therefore display multi-scale porosity and spatially varying macropores mimicking natural bone tissue. Gelatin nanoparticles were created through a two-step desolvation method, and BMP-2 was encapsulated into these nanoparticles using a diffusion method. The incorporation of BMP-2 encapsulated gelatin nanoparticles into PCL-HA scaffolds of uniform and FGSs was achieved through adsorption. Of particular significance, this study investigates the effect of morphology and BMP-2-gelatin nanoparticle (GNP) loading on biological and release performance of uniform and functionally graded scaffolds.

To study these effects, we conducted a thorough investigation of scaffolds made of Polycaprolactone (PCL) and Nanohydroxyapatite (HA) featuring macro-pore gradients in multiple directions. Furthermore, we present the incorporation of BMP-2 loaded GNPs into both uniform and FGSs produced through the NIPS process integrated to 3D printing, hence delivering scaffolds with multi-scale porosity. Using these scaffolds, our research presents an examination of the mechanical, biological and release performance by comparing PCL-HA uniform scaffolds with FGS scaffolds containing BMP-2 loaded gelatin nanoparticles. Experimental characterizations are carried out via mechanical UTM testing, imaging via micro-CT and scanning electron microscope (SEM), in-vitro testing including phalloidin and DAPI staining, alkaline phosphatase (ALP) activity and ELISA testing as well as confocal imaging.

3. Contributions

This thesis investigates the effect of morphology and BMP-2-gelatin nanoparticle (GNP) loading on biological and release performance of uniform and functionally graded scaffolds produced using 3D printing integrated to non-solvent induced phase separation (NIPS). NIPS was presented earlier to fabricate PCL-HA film scaffolds (Aydin et al., 2023) and recently integrated to 3D printing to fabricate FGSs with multi-scale porosity (Bilgili et al., 2024). As an extension, in this thesis we produce FGS using NIPS and 3D printing and integrate BMP-2 loaded GNPs to investigate their effect on the biological performance and BMP-2 release.

In summary, this thesis collectively contributes to:

1. Fabrication and characterisation of FGS 3D bone scaffolds via NIPS based 3D printing loaded with BMP-2 encapsulated GNPs.
2. Investigation of the potential of BMP-2 encapsulated GNP adsorption for controlled release of growth factors in PCL-nHA scaffolds.
3. A comprehensive exploration of the effects of porosity gradients on scaffold mechanical and biological performance.

Chapter 2

Background

2.1 Tissue Engineering

Injuries, diseases, and genetic defects cause damage to organs and tissues in millions of people. This causes healthcare and economic problems due to the limited regenerative capacity of human species. The current solution to overcome this problem is organ transplantation. Patient-derived autologous organs are used as the primary treatment. One limitation of this approach is the shortage of supply and the potential morbidity associated with donor sites. Alternative solutions include allograft organs and xenograft organs (Vo et al., 2012). Nevertheless, their utilization is constrained by the potential for disease transmission, host rejection, and infection hazards. The shortage of organ donors, low donor-recipient matches, and an aging population also make organ transplantation unsustainable and permanent (Chandra et al., 2020). At present, there is a waiting list of approximately 107,000 individuals in the United States who are in need of organ transplants (Lukin et al., 2022).

There has been a growing interest in tissue engineering as a way to address this critical medical need. It integrates concepts from biology, engineering, and medicine to develop tissues and organs that are functional (Figure 1). Tissue engineering aims to create functional tissues that can serve as substitutes for damaged or diseased tissues by replicating the extracellular matrix found in natural tissues (Ashammakhi et al., 2022). Tissue engineering is the process of creating three-dimensional tissues that mimic biological tissue using cells, scaffolds, and growth factors using different methods with multi-disciplinary functionality some of which are depicted in Figure 1.
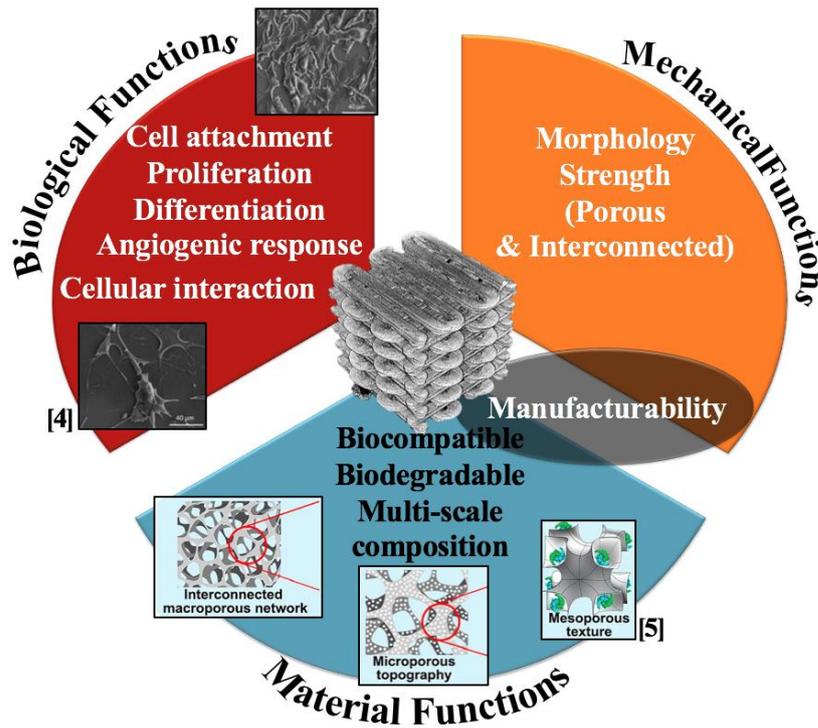
Figure 1. Multifunctionality requirement of tissue scaffolds

Maintaining the vitality and efficacy of the cells utilized in constructing these structures, ensuring that the structures are biocompatible, achieving vascularization, the process of creating new blood vessels within the artificial tissue that can integrate with the host tissue, and developing techniques for scaling up production of the structures are some of the key limitations in tissue engineering (Naderi et al., 2011).

2.2 Bone Tissue Engineering

Bone is a complex and dynamic tissue that serves several crucial roles, including mobility, mechanical support, and resistance to loads placed upon it by the human body. Structurally, bone comprises organic and inorganic constituents each playing a crucial role in its structure and function. Inorganic components, mainly calcium and phosphate, provide rigidity and hardness, while the organic components consist mainly of collagen, which provides resilience and durability to the bone. Bone can be examined as compact bone and trabecular bone. The periosteum, also known as the outer layer of bone, serves as a protective shield for the bone structure. The compact bone, located underneath the periosteum, is characterized by its dense and rigid structure, constituting the majority of the bone's overall mass. Within the compact bone are small channels that contain blood

vessels and nerves, which nourish the bone tissue and provide sensory feedback. The trabecular bone, also known as the inner portion of the bone, consists of a complex arrangement of delicate and interconnected trabeculae. Trabecular bone, although less dense compared to compact bone, still possesses considerable strength, and plays a crucial role in providing support to the bone structure. Within the spaces present between the trabeculae, bone marrow is found, responsible for the production of both red and white blood cells (Wang et al., 2016). Physiology of bone is shown in Figure 2 demonstrating its main components.
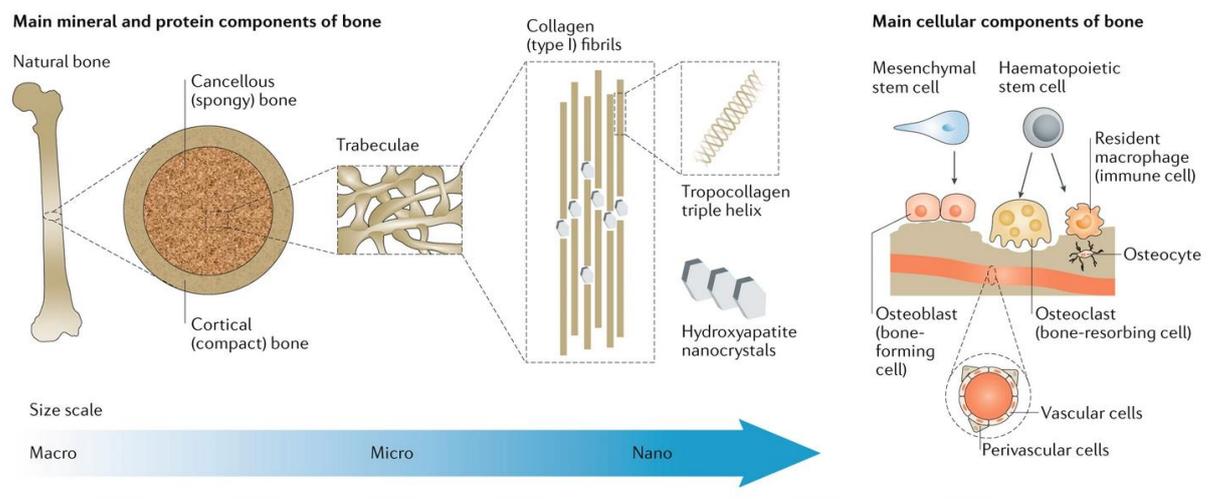
Figure 2. Physiology of bone (Koons et al., 2020b)

Bone possesses the remarkable ability to undergo self-healing, although the extent of this healing process depends on the severity of the fracture (Awad et al., 2014). When fractures exceed a critical size threshold, typically around 2 cm, the natural healing capacity of bone may require external assistance (Koons et al., 2020b). There are different strategies to help the bone to heal such as using bone autografts, allografts, or implants. However, these approaches are not without their limitations. Autografts may lead to issues like donor site morbidity, infections, or increased blood loss (Roberts & Rosenbaum, 2012). Similarly, the utilisation of allografts carries the risk of infection transmission and host rejection. Implants, on the other hand, may be prone to corrosion, toxicity, (T. Kim et al., 2020) or necessitate additional surgical interventions. In order to alter these limitations, bone tissue engineering strategies have been developed (Maia et al., 2022a).

In short, an emerging field of regenerative medicine has been bone tissue engineering, which develops strategies for repairing or regenerating damaged bone tissue. The primary

goal is to restore the structure, function, and mechanical integrity of damaged or diseased bones. It is fair to state that bone tissue engineering can be examined in three main categories: cells, scaffolds, and bioactive molecules (Awad et al., 2014).

2.2.1 Cell Types in Bone Tissue Engineering

The traditional approach in tissue engineering uses cells from tissues planted on scaffolds. The cells may originate from autologous, allogeneic, or xenogeneic sources. Autogenic cells are easier to manipulate and can reduce the risk of causing an immune response when implanted into a patient and these cells eliminate the need for immunosuppressants. Therefore, they are the primary choice in the current state (Al-Himdani et al., 2017).

The categorization of cells used in tissue engineering, such as, adult somatic cells, stem cells and progenitor cells, is determined by their ability to differentiate (Figure 3). Stem cells possess the remarkable ability to transform into specific cell types required for the regeneration and restoration of damaged tissues. These cells are characterized by their non-specialized nature, enabling them to adapt and differentiate into the precise cell types necessary for tissue repair (Al-Himdani et al., 2017). Stem cells are categorized based on their differentiation capabilities into totipotent, pluripotent, multipotent, and unipotent cells. Totipotent cells, in addition to being able to differentiate into any cell type, also possess the unique ability to develop into a complete organism. Pluripotent stem cells possess the remarkable ability to differentiate into various types of fetal or adult cells, yet they lack the capacity to develop into embryos. Multipotent stem cells possess the capacity to undergo differentiation into a restricted range of cell types. Unipotent cells are the cells that could turn into a single cell type (Loya, 2014). Stem cells can be categorized into two main types according to their source: embryonic stem cells and tissue-derived stem cells. Embryonic stem cells (ESC) are derived from the early stages of embryo formation and possess the ability to develop into various cell types. The drawback of using embryonic stem cells is that the distinction between ESC and the other stem cells or cancer cells is difficult. Tissue derived stem cells have subtypes such as: fetal stem cells and adult stem cells. Adult stem cells include induced pluripotent stem cells (iPS), induced tissue-specific stem cells (iTS), and mesenchymal stem cells (Ntege et al., 2020). Various organs within the adult body, such as the bone marrow, liver, and blood, among others, serve as sources for adult stem cells. Using adult stem cells is

preferable because they do not cause immunological response. Despite this, their use is limited due to decreasing quality and quantity of cells with age (Łos et al., 2019).

In contrast to adult cells, progenitor cells are more differentiated and considered multipotent instead of pluripotent. Due to their full differentiation, adult somatic cells have limited future differentiation potential and relatively low growth rates (Al-Himdani et al., 2017).

In bone tissue engineering, the objective is to develop innovative therapies for bone regeneration and repair by comprehending the distinct characteristics and functions of various cell types.
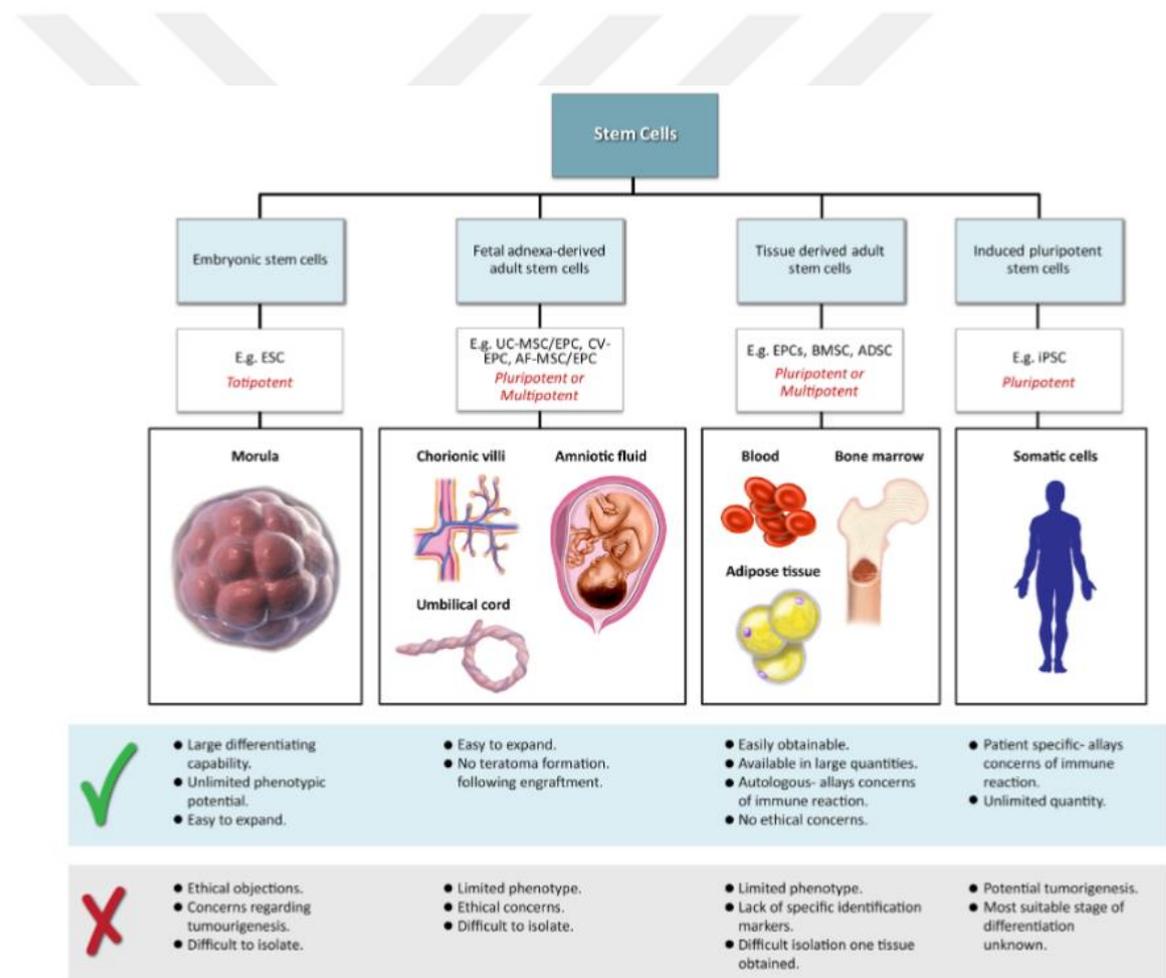
Figure 3. Different cell sources employed in tissue engineering (Al-Himdani et al., 2017)

2.2.2　Materials in Bone Tissue Engineering

The choice of materials utilized is a critical factor in the field of bone tissue engineering. The materials utilized should ideally be biocompatible, ensuring that they do not provoke any negative responses from the immune system, and should also have osteoinductive and osteoconductive features. The process of osteoconduction involves migrating osteoinducible cellular elements (osteoblasts, osteoclasts) into the scaffolds, along with their supplementary vasculature. Osteoinductivity describes the process of transforming different lineages of cells into osteogenic cells. A variety of different materials used in bone scaffolds have their specific properties that affect osteoinduction and osteoconduction (Ghassemi et al., 2018). Materials frequently utilized in bone tissue engineering are typically classified into polymers, ceramics, composite materials, and metals.

The distinctive mechanical properties of metal make it an appealing material for use in bone tissue engineering. Metals are constrained in their application as scaffold materials due to their properties such as corrosion. The majority of metals, including tantalum, titanium, and titanium alloys, exhibit non-biodegradable properties. Moreover, magnesium carries the possibility of toxicity as a result of the release of metal ions (H. Qu et al., 2019).

Polymers are organic materials composed of repeating subunits. There is a wide range of polymers utilized in tissue engineering, including both synthetic and natural variants. Natural polymers, including gelatin, chitosan, alginate, collagen and cellulose, are derived from biological sources. Natural polymers show excellent biocompatibility and degradation features. Tissue engineering applications find these materials desirable due to their origin from sustainable sources, typically hydrophilic nature, ability to form hydrogels, and promotion of cell attachment. Collagen is primary protein in natural bone, and it consists of amino-acid sequences that enable cells to easily attach to the bone matrix. They have a use as microparticles or nanoparticles that deliver other molecules. However, they have low mechanical strength, and acquiring and processing these polymers from living organisms creates compositional variability in different batches (Koons et al., 2020b), and they have low tunability (Reddy et al., 2021). These drawbacks limit their application in tissue engineering and motivate to use composites mostly in the form of mixtures of ceramics and polymers.

Synthetic polymers present a vast array of chemical alterations that can be adjusted to fulfil specific requirements, providing greater possibilities for customization. In contrast, in comparison to natural polymers, synthetic polymers exhibit diminished bioactivity, lack of cellular recognition sites, and limited osteoconductivity. In the creation of scaffolds, several types of synthetic polymers have been studied. Among them, the aliphatic polyesters, namely Poly(ε-caprolactone) (PCL), Poly(lactide-co-glycolide) (PLGA), and polylactide (PDLA, PLLA), are widely recognized as the most employed synthetic polymers (Donnaloja et al., 2020a).

The absence of bioactivity in synthetic polymers and the predominant inorganic composition of bone structure (Feng, 2009), incorporating hydroxyapatite into the scaffold increases the chances of enhancing bioactivity and promoting better integration with the natural bone tissue. In this thesis, due to its favourable properties and our earlier expertise we make use of PCL- HA composites.

The choice of materials is essential for the success of bone tissue engineering and subsequent bone repair or replacement procedures. The viability of utilizing these materials has been established for the fabrication of NIPS integrated to 3D printing in earlier studies and producing FGSs mimicking bone like tissue morphology.

2.2.3 Scaffolds in Bone Tissue Engineering

Scaffolds represent a fundamental component of bone tissue engineering, alongside cells and signalling molecules. These scaffolds are intricate three-dimensional (3D) structures designed to imitate the native bone tissue's extracellular matrix (ECM) (Buer Boyetey et al., 2023). There are certain requirements of a scaffold to be an ideal support for the regeneration of bone tissues, such as biocompatibility, biodegradability, and osteoconductivity (Bahraminasab, 2020). To ensure a successful integration between the body and the scaffold, it's crucial that scaffolds degrade slowly and in a controlled manner over time, and it should be in the rate of the natural bone growth (Tang et al., 2016). A scaffold must provide a substrate for cellular adhesion and should stimulate the growth of the cells (Ghassemi et al., 2018).

Porosity is one of the most crucial properties of a scaffold. Interconnected pores are required for cells to colonize scaffolds and infiltrate inner parts. Also, it is essential to ensure the transportation of the nutrients, metabolic wastes, and gases through the scaffold. It has been suggested that an interconnected porosity of approximately 90% is

suitable to ensure effective interactions between cells and biomaterials (Donnaloja et al., 2020b). Additionally, porosity has an important effect on mechanical characteristics of the scaffold. According to previous studies, as porosity increases, elastic modulus storage modulus decreases (Hollister, 2009).

Osteoblasts require a larger pore size when forming new bone, as they naturally range in size from 10-50 microns, up to 100-200 microns when regenerating mineralised bone (Abbasi et al., 2020). Also, a scaffold must exhibit mechanical characteristics of the native bone tissue. Bone tissue possesses a modulus of elasticity of 18 GPa when applied axially, 12 GPa when applied transversely, and 3.3 GPa when subjected to shear stresses (Donnaloja et al., 2020b).

The design of scaffolds holds great significance in delivering the required functionality for effective bone regeneration via tuning their properties among which material and geometrical composition stands out. Nature displays a plethora of graded patterns, from the complex trabecular formations in bones to the unique variations in seashells and plants (Li et al., 2020). These organic patterns have influenced the innovation of Functionally Graded Structures (FGS), which have remarkable attributes like enhanced porosity, tailorable stiffness, superior energy absorption, and a constructive interaction with biological tissues. Through a nuanced distribution of mechanical and biological features, FGS can correctly address the biomechanical needs of bone tissue repair and regrowth. Moreover, by finely tuning the arrangement of varying-sized pores, FGS can emulate the structure and mechanical traits of natural bones. Diverse techniques have emerged to craft these structures, considering both their mechanical and biological functionalities (Zhou et al., 2020). For example, integrating natural or man-made scaffolds with progressive gradients in attributes like shape, rigidity, porosity, and density can emulate the characteristics of the Extracellular Matrix (ECM), amplifying the therapeutic promise for tissue restoration (Pattnaik et al., 2023). *In this thesis, with the proved importance of multi-scale micro and macroporosity of bone scaffolds, we fabricate scaffolds with micropores within the extruded filament via NIPS and a controlled macro-porosity with variations both in the radial and longitudinal directions through 3D printing. Within these promising 3D functionally graded scaffolds created using the NIPS method integrated with a 3D extrusion-based printer, we further load these with BMP-2 encapsulated gelatin nanoparticles and analyse the impact of morphology and BMP-2 loaded gelatin nanoparticles on their biological performance in-vitro.*

2.2.4 Methods Used for Scaffold Fabrication

Different scaffold fabrication techniques can yield scaffolds with varying properties, including porosity, mechanical strength, degradation, and cell compatibility. When selecting a fabrication method, it is important to consider the intended goal of the scaffold. There are several methods available for fabricating porous 3D scaffolds, such as freeze-drying, electrospinning, gas foaming, solvent casting, nonsolvent induced phase separation (NIPS) (Yanar et al., 2020) and particulate leaching (Vesvoranan et al., 2022). These methods suffer from a lack of precision in regulating the scaffold's structure, including pore size, pore geometry, large-scale reproducibility which is vital in achieving patient specific multi-functional scaffolds.

3D printing, which is also referred to as additive manufacturing, has the potential to precisely control the structure of the scaffold, in a way that can be more reproducible in substantial amounts (Maia et al., 2022a). 3D printing enables the production of complicated topological characteristics, thereby facilitating the development of personalised scaffolds designed to meet unique needs of individual patients. The most common types of 3D printing are fused deposition modelling (FDM), extrusion, selective laser sintering (SLS), inkjet printing, stereolithography (SLA) as shown in Figure 4. Filaments in extrusion-based 3D printing are formed by extruding material through a nozzle using pneumatic pressure or a mechanical plunger. Subsequently, these filaments are laid down in a layer-by-layer fashion (Koons et al., 2020a).

Unlike 3D printing, NIPS is commonly employed as a method to fabricate polymeric membranes, where non-solvents are utilised to induce phase separation. This technique allows for the creation of microporous membranes(Kahrs & Schwellenbach, 2020). By combining the NIPS process with 3D printing, it is possible to fabricate 3D scaffolds with precisely controlled microporosity (J. W. Kim et al., 2017b; Seok et al., 2020). *In this thesis, we integrate NIPS to 3D printing as was done earlier to produce FGSs and in particular incorporate BMP-2 encapsulated GNPs to allow for further functionalization assessed through their potential for controlled growth factor release.*
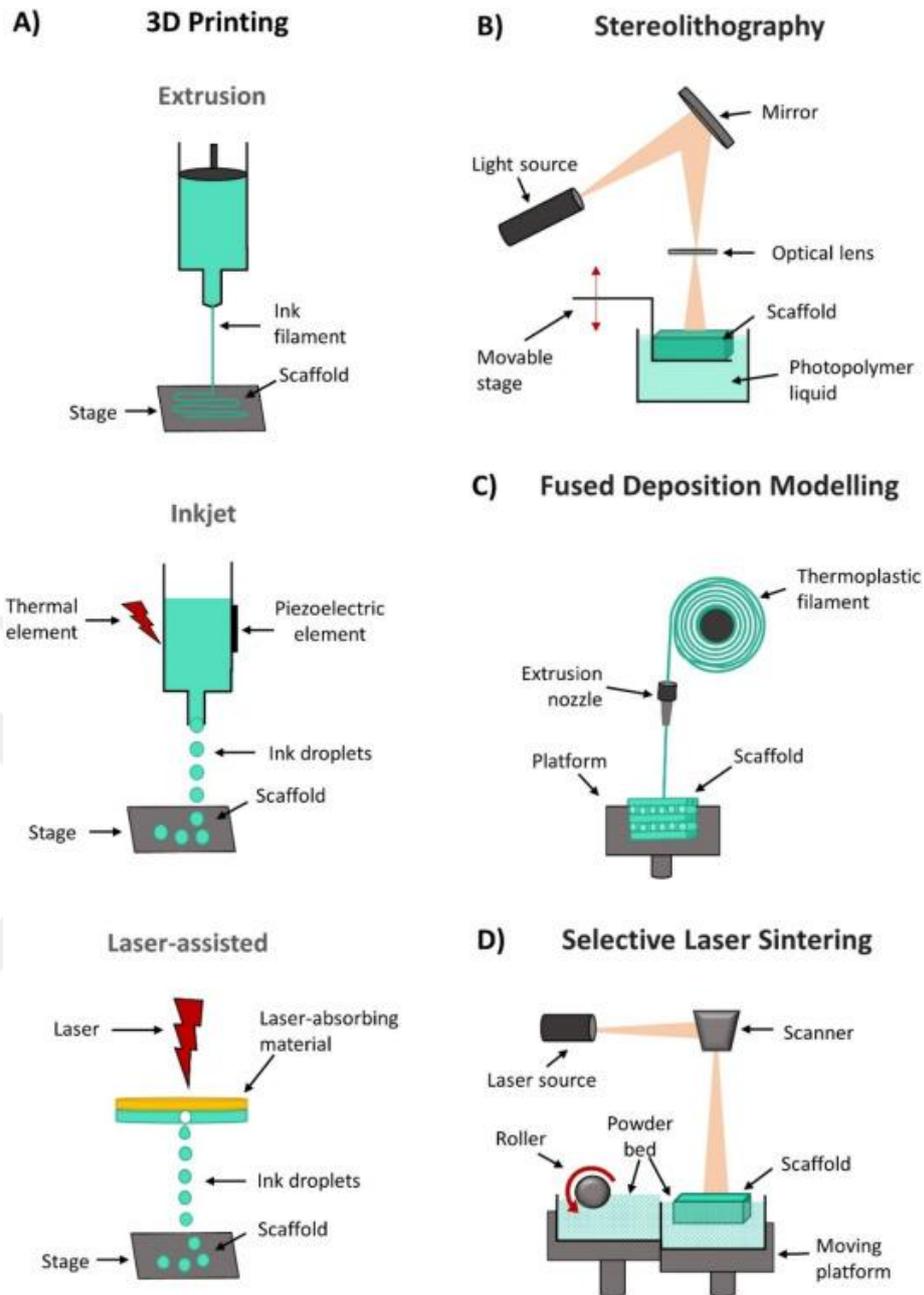
Figure 4. Additive manufacturing methods: A) Extrusion, inkjet, laser assisted printing, B) Stereolithography, C) Fused deposition modelling, and D) Selective laser sintering (Maia et al., 2022b).

2.2.5 Bioactive Molecules in Bone Tissue Engineering

The healing process of a bone fracture involves the coordination of various bioactive molecules that orchestrate vital mechanisms such as cellular growth and specialization (Szwed-Georgiou et al., 2023). Notably, growth factors are significantly important in promoting the regeneration of tissues. To emulate this natural process, an optimal tissue scaffold should effectively manage the localised and targeted delivery of growth factors

and regulate the timing of growth factor release. In the context of osteogenesis and bone healing, osteoinductive growth factors, including but not limited to bone morphogenetic proteins (BMPs), transforming growth factors (TGF-β), insulin-like growth factors (IGF), vascular endothelial growth factors (VEGF) play a regulatory role in guiding cellular behaviour (Oliveira et al., 2021).

The short protein half-life, rapid degradation, and enzyme-mediated deactivation of growth factors necessitate a carrier for *in vivo* applications. It is possible to deliver growth factor-containing scaffolds through physical entrapment, covalent or noncovalent binding, or by using micro- or nanoparticles as reservoirs for growth factors (De Witte et al., 2018). A wide array of synthetic and natural polymers has been employed for encapsulating growth factors within polymeric micro- or nanoparticles. Due to varying surface-to-volume ratios, the size of polymer particles directly influences the rate of protein release (Tayalia & Mooney, 2009). Polymers or inorganic materials such as PLGA, PHBV, PLG, HA, silica, chitosan, gelatin are widely studied for growth factor delivery (Chen et al., 2007; Choe et al., 2022; Neumann et al., 2013; Schrade et al., 2022; Xie et al., 2010; Yilgor et al., 2009).

Gelatin nanoparticles have emerged as promising carriers among these options, owing to their biocompatibility, biodegradability, and customizable properties. Studies exist on the encapsulation of BMP-2 within gelatin nanoparticles demonstrating its potential to offer controlled and sustained release, promoting prolonged therapeutic effects. The unique characteristics of gelatin nanoparticles make them an attractive option for delivering BMP-2. For instance, to achieve controlled release of growth factors, Wang et al. prepared BMP-2 and ALP loaded gelatin nanospheres and microspheres and investigated the properties of nano and micro-sphered gelatin gels (H. Wang et al., 2012). In their study, Xia et al. created scaffolds using BMP-2 loaded gelatin microspheres with PLGA and examined how these scaffolds influenced osteogenesis (Xia et al., 2019). Poldervaart et al. explored the bioprinting of hydrogel scaffolds incorporating controlled-release particles containing BMP-2. The research investigated whether the sustained presence of BMP-2 within scaffolds enhances osteogenic differentiation and bone formation in comparison to rapid growth factor release (Poldervaart et al., 2013). However, majority of these studies focused on scaffolds with micro-porosity or structures with uniform pore morphology. *To the best of our knowledge, no study exists investigating BMP-2 loaded gelatin nanoparticle release kinetics from scaffolds with FGS morphologies mimicking the actual bone structure. To address this gap in the literature, in this thesis GNPs were*

synthesized for BMP-2 growth factor encapsulation and incorporated into both uniform and FGSs for a comparative analysis in their in-vitro and release behaviour.

2.2.5.1 Encapsulation of Bioactive Factors

Particulate encapsulation involves the incorporation of bioactive substances into nanoparticles or microparticles made of natural biodegradable materials like collagen, alginate, and gelatin (Caballero Aguilar et al., 2019). Various techniques such as electrospinning, template assembly, and casting are utilized in this delivery method (Zhang & King, 2020). These encapsulated substances are then incorporated into scaffolds to target bone defects. The release mechanism of this approach includes the diffusion of bioactive factors, degradation of nanoparticles or microspheres, and scaffold degradation.

There are numerous advantages associated with the use of nanoparticles or microparticles within scaffolds. Firstly, the small size, large surface area, and high porosity of these particles enhance cell adhesion and proliferation, while also significantly improving the loading rates of bioactive factors (Tarhini et al., 2017). Secondly, the incorporation of nanoparticles or microparticles helps to mitigate the degradation of bioactive factors by enzymes, thereby enhancing the efficacy of bone regeneration. Lastly, this approach enables the simultaneous loading of multiple types of bioactive factors and allows for the regulation of their release (Subbiah & Guldberg, 2019).

2.2.5.2 Bioactive Factors' Release Mechanism

Understanding the mechanisms that control the release of bioactive substances is crucial for improving continuous-release platforms and enhancing bone regeneration. These mechanisms include diffusion, degradation, and reactions to stimuli such as pH, temperature, and enzymes as shown schematically in Figure 5. Bioactive Factors' release mechanism a) responsive to stimuli: pH, temperature, and enzymes. b) degradation c) diffusion (Pei et al., 2023).
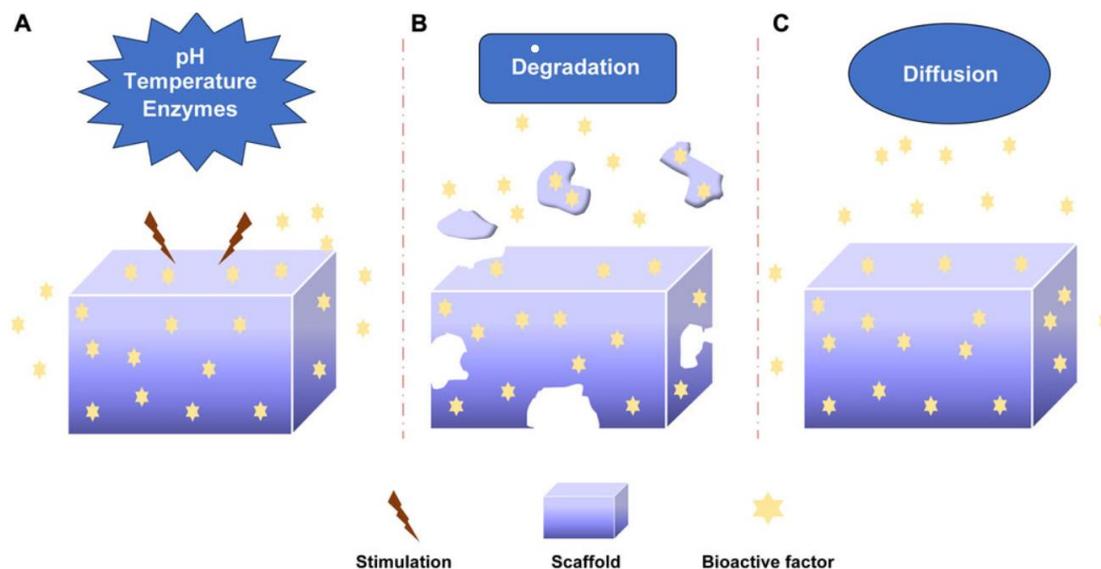
Figure 5. Bioactive Factors' release mechanism a) responsive to stimuli: pH, temperature, and enzymes. b) degradation c) diffusion (Pei et al., 2023).

Various environments with different levels of acidity or alkalinity can have an impact on the release of bioactive substances due to the varying conditions found within organs, tissues, and cells. When pH levels in the surrounding environment change, pH-sensitive materials release bioactive substances as ionizable groups or acid-cleavable bonds are broken. (M. Qu et al., 2020). This sensitivity is made possible by the absorption or release of protons, which can lead to changes in the swelling, contraction, and other characteristics of biomaterials. For example, the weak polyelectrolyte poly (allylamine hydrochloride) experiences an increase in osmotic pressure as the pH decreases, thereby facilitating the diffusion of bioactive substances (Pei et al., 2023).

2.2.5.3 Release with Degradation

The release of bioactive factors can occur through the degradation of carrier materials. When biological materials undergo hydrolysis or other forms of degradation, the bioactive factors are released. The sustained-release rate of bioactive factors is influenced by the degradation rate of the biological materials (Pei et al., 2023).

2.2.5.4 Diffusional Release

The bioactive components diffused out of the porous framework of bioactive substances due to a concentration gradient, moving from areas of high concentration to areas of low concentration. The rate at which diffusion takes place was influenced by the size, porosity, and interconnectedness of the pores (Pei et al., 2023).

2.2.6   Gelatin Nanoparticle Preparation Techniques

Gelatin nanoparticles can be generated using different methods, such as de-solvation, emulsification-solvent evaporation, reverse-phase microemulsion, coacervation-phase separation and nanoprecipitation. In the coacervation method as depicted in Figure 6, following the separation of liquid-liquid phases, the polymer precipitates within the solution, giving rise to two distinct and immiscible phases. Typically, natural salts like sodium chloride or sodium sulphate, as well as alcohols like ethanol, are employed to achieve the formation of nanoparticles (NPs). However, an alternative approach known as complex coacervation involves the utilization of macromolecules, such as proteins or polyelectrolytes, that have opposite charges. The dehydration of gelatin molecules ultimately leads to the creation of gelatin nanoparticles (GNPs), which can be further cross-linked with other agents like GA.
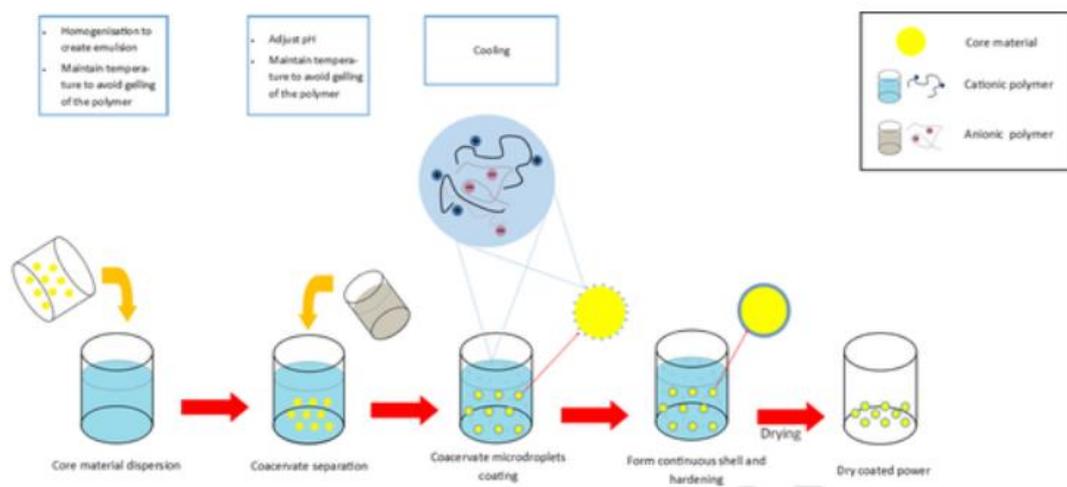
Figure 6. Schematic representation of complex coacervation method (Dhakal & He, 2020)

The formation of GNPs can be achieved through the utilization of the solvent evaporation technique as graphically shown in Figure 7, which involves the use of either single emulsions or double emulsions. During this procedure, gelatin and medications found in the water-based layer are carefully blended with the oil-based layer, which can consist of either polymethyl methacrylate or paraffin oil. Subsequently, the resulting mixture is cross-linked using either GA or genipin. Afterwards, the solvent is evaporated, leading to the solidification of the nanoparticles (NPs).
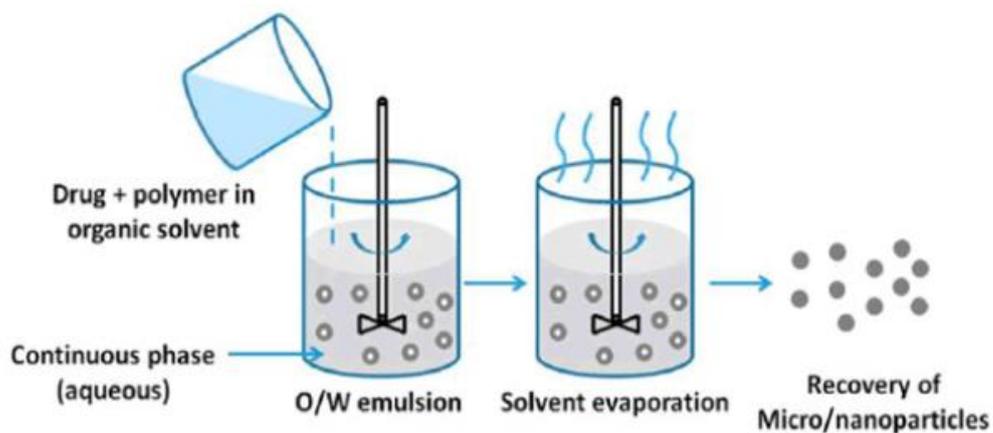
Figure 7. Representation of solvent evaporation technique (Rao & Kamala Kumari, 2020)

The process of creating microemulsion as summarized in Figure 8 involves the introduction of an aqueous gelatin solution into a surfactant solution containing sodium bis(2-ethylhexyl) sulfosuccinate, within n-hexane. This mixture is then cross-linked with GA and the n-hexane is subsequently evaporated, resulting in the recovery of GNPs. The utilization of microemulsion offers several benefits due to its ability to provide precise manipulation of nanoparticle size.
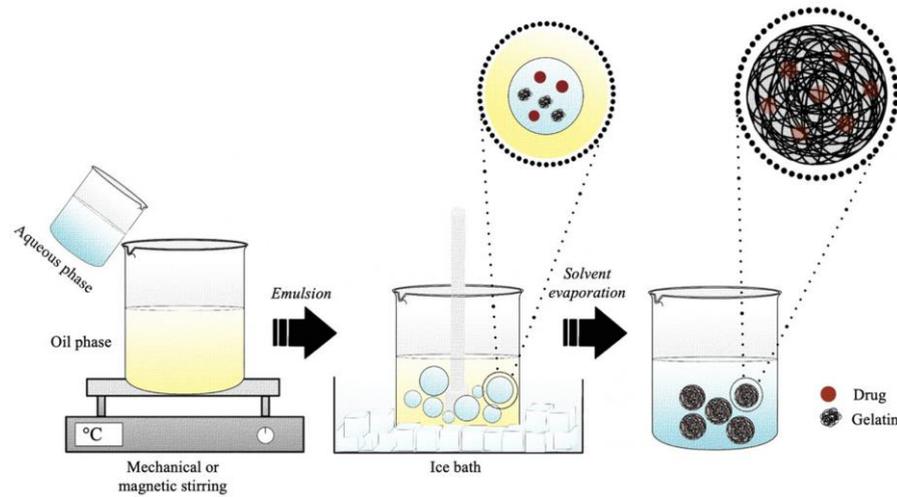
Figure 8. Water-in-oil emulsion technique (Milano et al., 2023)

The nanoprecipitation method shown in Figure 9 includes dissolving gelatin in a water-based solvent phase. The aqueous phase is mixed with ethanol, which acts as the nonsolvent phase, and includes poloxamer as a stabilizing agent. The generation of gelatin nanoparticles occurs at the interface between water and ethanol, facilitated by solvent displacement-induced interfacial turbulence. Following this, the formed GNPs are cross-linked using glutaraldehyde (GA).
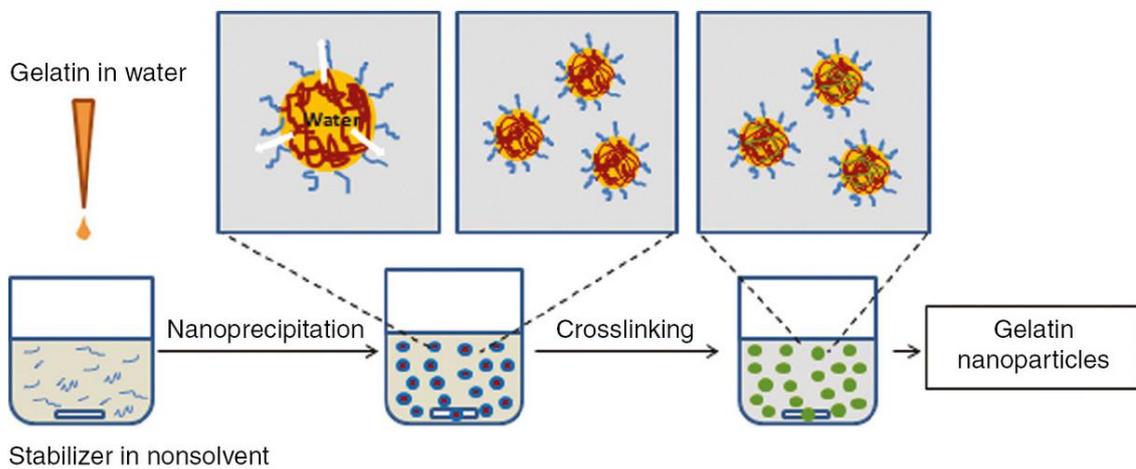
Figure 9. Schematic representation of nanoprecipitation method (Yasmin et al., 2017)

The two-step desolvation method as shown in Figure 10 consists of introducing a desolvating agent into an aqueous gelatin solution to eliminate water and dehydrate the gelatin molecules. Subsequently, the low molecular weight gelatin is eliminated, leaving only the high molecular weight fraction. This residual gelatin is then dissolved in water, and acetone is gradually added to the solution while maintaining a regulated pH. To

achieve uniformly hardened spherical nanoparticles, a cross-linking agent is introduced. The purification process entails thorough centrifugation (Yasmin et al., 2017). *This thesis employs the two-step desolvation method for gelatin nanoparticle production, chosen for its ability to generate smaller and more uniform nanoparticles. This method involves selectively eliminating low molecular weight gelatin, enabling precise control over particle size and results in a more uniform distribution.*
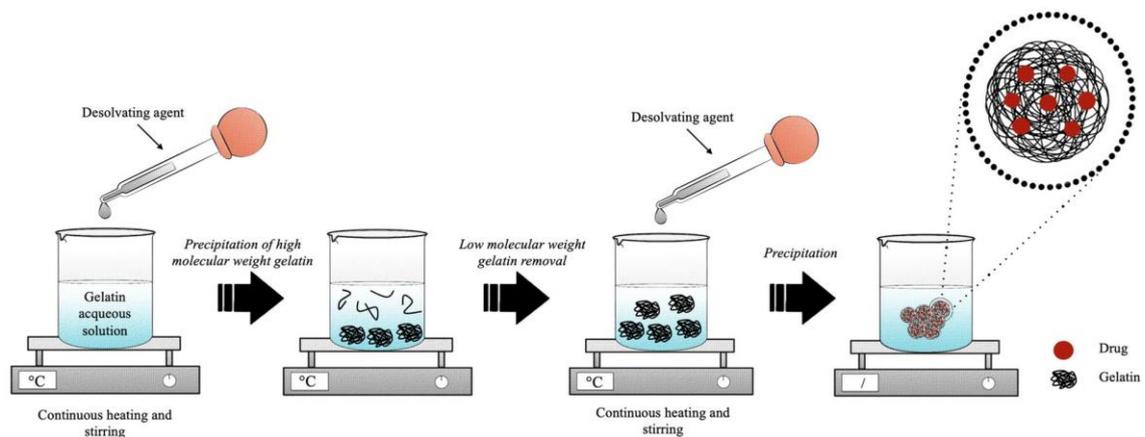
Figure 10. Schematic representation of two-step desolvation method used in this thesis to produce gelatin nanoparticles (Milano et al., 2023)

Chapter 3

Material and Methods

Within this chapter, we outline the materials and methods of the primary approach utilized in the creation of scaffolds and gelatin NP synthesis, along with the process of loading BMP-2 growth factors. A schematic representation of the entire process used in this thesis is shown in Figure 13. We also discuss the characterization methods employed in this thesis including porosity analysis using micro-CT, scanning electron microscopy for morphology analysis, evaluation of mechanical properties, viscosity analysis, measurement of contact angle, and in vitro testing methods such as MTS assay for cell viability assessment, ALP assay for alkaline phosphatase activity measurement, ELISA for release studies and confocal imaging for morphological analysis.

3.1 Materials

Poly(ε-caprolactone) pellets (PCL, M_n = 80.000), nanohydroxyapatite powder (nHA, <200 nm), glutaraldehyde (GA, 50 wt% solution in water), gelatin (type A, bloom 300 from bovine skin) were obtained from Sigma Aldrich (St. Louis, MO, USA). Acetone and tetrahydrofuran were purchased from Merck. Glycine was purchased from Neofroxx. The experiments were conducted using Millipore water having a resistivity of 18.2 MΩ·cm. Cell culture materials constitute MC3T3-E1 subclone 4 (ATCC CRL-2593) cells, Alpha-MEM (Gibco) medium, Fetal Bovine Serum (Pan Biotech), Penicillin-Streptomycin solution (Pan Biotech). For in vitro assays MTS assay (CellTiter 96 Aqueous One Solution Cell Proliferation Assay, Promega), ALP assay kit (Alkaline Phosphatase, Diethanolamine Detection Kit, Sigma Aldrich), M-PER (Mammalian Protein Extraction Reagent, Thermo Scientific) were used. For staining the actin filaments, Alexa Fluor 546 Phalloidin dye (Invitrogen) was used, and for staining the nucleus of the cells DAPI (Sigma) was used.

3.2 Preparation of Solution

PCL pellets were dissolved in THF at 40 °C with the aid of a magnetic stirrer and a water bath to prepare solutions for 3D printing. The gradual addition was done at a concentration of 15% w/v. After overnight stirring, nHA powder was gradually added to the solution (10% with respect to PCL) and stirred for 24 hours. Since THF is an easily evaporating solvent, it is important to carefully seal the solution beaker in all the steps.
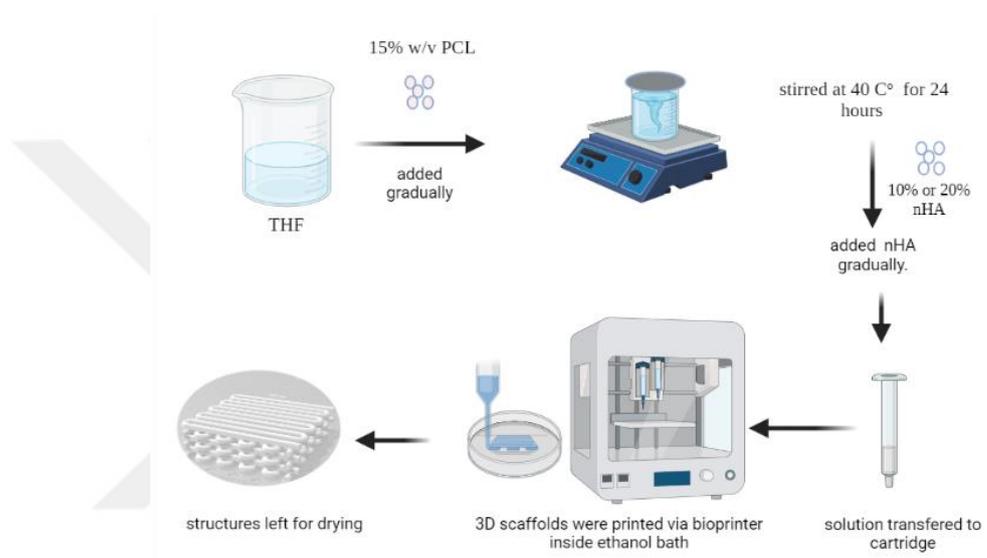
Figure 11. Schematic representation of NIPS based 3D printing used in this thesis (Bilgili et al., 2024).

3.3 Scaffold Fabrication

The solution was directly extruded from the print head to an ethanol (70%) bath in order to integrate the 3D printing process with the NIPS process. A pneumatic extrusion-based 3D bioprinter Inkredible (Cellink, Gothenburg, Sweden) was used for fabricating the uniform and FGS scaffolds with the morphologies shown in Figure 12. CURA (Version 5.6.0, Ultimaker) was used to generate G-code from predesigned SOLIDWORKS models. In order to build the scaffolds, using a layer-by-layer extrusion of the ink, this G-code was used to control the relative positioning of the workstation and the nozzle.

The composite solution, once prepared, was loaded into the barrel, and extruded using a pneumatic system. Printing occurred with the nozzle submerged in an ethanol bath. The nozzle size of 25G was used to create uniform and FGS scaffolds with 0.4-0.6 strut sizes.

The integration of 3D printing and the NIPS method involved adjusting key parameters: pneumatic pressure level, printing speed, and layer thickness. Optimization of these settings was based on the viscosity of the solution.

In this thesis, the pressure for uniform scaffolds was adjusted to 140 kPa, while the nozzle speed was set at 10 mm/s for the initial layer and 15 mm/s for the subsequent layers. On the other hand, for FGS scaffolds, the pressure was set to 170 kPa, with the first layer's speed set at 8 mm/s and the remaining layers at 16 mm/s. The variation in speed between the first layer and the subsequent layers was due to the curing process of the solution. If the speed is too low for all layers, the first layer cures too quickly, causing the scaffold to detach from the glass surface. Conversely, if the speed is too fast, the first layer fails to adhere to the glass surface.

CAD Images	Uniform	FGS
Transverse View		
Coronal View		
Stl File Structure Size	10.5 x 10.5 x 3.0 mm	14.08 x 14.08 x 3.59 mm
Measured Scaffold Size	8.74 x 8.67 x 2.81mm	13.25 x 12.55 x 3.23 mm
Relative Change % (x, y, z)	16.76, 17.43, 6.33	5.89, 10.87, 10.03
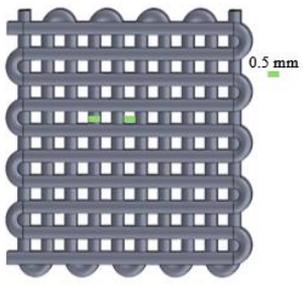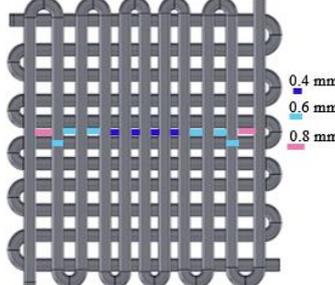
Figure 12. Designs and dimensions of FGS and uniform scaffolds

3.4 Preparation of Gelatin Nanoparticles and BMP-2 loaded Gelatin Containing Scaffolds

We prepared gelatin nanoparticles using an existing method of two-step desolvation described by Coester et al. (Coester et al., 2000) for which the steps are given as follows.

1. A solution was prepared by dissolving 1.25 g of gelatin in 25 ml of ultrapure water at a temperature of 50 °C for 30 minutes. Subsequently, the solution was taken off the heat and 25 ml of cold acetone was added. The mixture was then allowed to sit at room temperature for 1 hour, leading to the precipitation of the high molecular weight fraction.

2. The supernatant is discarded, and the remaining gelatin was redissolved in ultrapure water (25 ml) at 50 °C for 30 minutes.

3. The dissolved solution is cooled to room temperature and the pH is adjusted to ~2.5 (5 M HCl).

4. Chilled acetone was added to the solution dropwise (2 ml/min, 1000 rpm) at 40 °C until the Tyndall effect was observed (~75 ml acetone).

5. The nanoparticles were crosslinked with glutaraldehyde (25%, 165 μl) overnight.

6. After crosslinking, glycine solution (100 mM) was added to the nanoparticle suspension to block the unreacted aldehyde groups of glutaraldehyde and stop the crosslinking reaction.

7. The nanoparticles were washed by centrifugation (16,500 xg, +4 °C, 30 minutes) three times and redispersed in water and freeze dried.

Diffusional loading was used as a technique to enhance the loading of BMP-2 onto gelatin nanoparticles. This method involved directly combining a protein solution with freeze-dried gelatin nanoparticles. The dosage of BMP-2 loaded to gelation nanoparticles is 50 ng BMP-2 in 100 μl for 1 mg of gelatin nanoparticle. To ensure complete absorption of BMP-2, the combined solution was stored at a temperature of 4 °C for a period of 20 hours. After incubation period, BMP-2 loaded GNPs were centrifuged at 16,500 xg, +4 °C, 10 minutes. The supernatant part was collected as non-entrapped BMP-2, and the pellet was resuspended in the same amount of PBS. BMP-2 incorporation efficiency is calculated using ELISA test, the non-entrapped part was measured with other samples collected during the release study at specific time intervals. Calculation was made using following equation.

$$\text{Incorporation Efficiency (IE\%)} = \frac{\text{Practical Loading}}{\text{Theoretical Loading}} \times 100$$

Here the practical loading refers to the value obtained from ELISA test and the theoretical loading corresponds to the initial amount that was originally added to the solution, namely 50 ng of BMP-2.

1 mg of BMP-2 loaded nanoparticles were introduced into the uniform and FGS scaffolds. Specifically, a nanoparticle solution containing 1 mg in 100 μl was applied to the scaffolds and allowed to incubate for a duration of 2 hours at a temperature of 37 °C. Subsequent to the incubation phase, cell culture and studies were conducted.
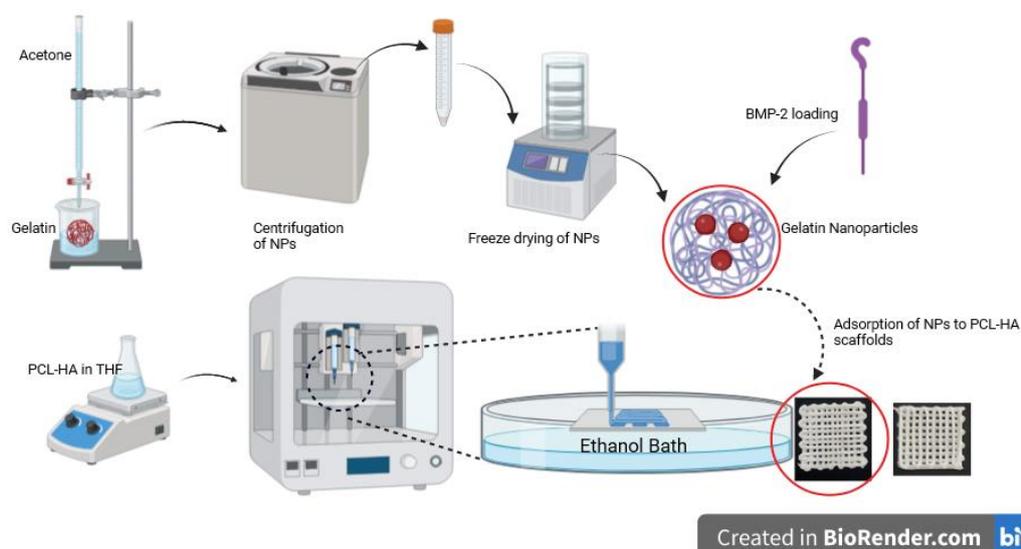
Figure 13. Schematic representation of experimental process used to fabricate scaffolds and incorporate BMP-2 loaded GNPs produced using two step desolvation technique, contribution of thesis is encircled. The figure was drawn by using BioRender.com.
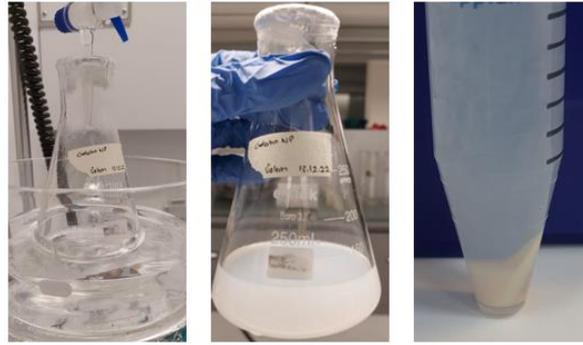
Figure 14. Nanoparticle preparation process using two-step desolvation. From left to right: 1. Gelatin desolvation in ultrapure water. 2. Observed Tyndall effect. 3. Nanoparticles after centrifuge.

3.5 Characterization of the Scaffolds

3.5.1 Morphological Analysis with Micro-CT

The assessment of scaffold morphology, consisting of total porosity and pore size distributions, was conducted through Micro-CT (SkyScan 1172; Bruker, Belgium). Following the scanning procedure, 2D slices underwent reconstruction into a 3D structure using the Skyscan NRecon (Version 1.7.5.4) software. Morphological images of the specimens from various cross-section slices were generated using the DataViewer program. For 3D morphological analysis, the CTAn software (SkyScan) was employed. To ensure uniformity, a round-shaped region of interest (ROI) was applied to 101 selected slices, establishing a consistent volume of interest (VOI). Subsequently, the original CT image underwent conversion into a binary image, with lower and higher grayscale threshold values have been set to automatic and 255, correspondingly. The parameters utilised for scaffold analysis are given in Table 1. Scanning parameters used for imaging using micro-CT SkyScan 1172 tomography device..

Table 1. Scanning parameters used for imaging using micro-CT SkyScan 1172 tomography device.

	Camera Pixel Size (μm)	Resolution in Pixels	Image Pixel Size (μm)	Source Voltage (V)	Exposure Time (ms)	Rotation Step (degree)	Filter
Uniform	8.15	1336 x 2000	12.95	60	150	0.4	None
FGS	12.95	1336 x 2000	12.95	60	280	0.4	None

3.5.2 Scanning Electron Microscopy Imaging

Scanning Electron Microscopy Imaging (Zeiss Leo Supra VP 35 field emission) was used to examine the nanoparticles and cell morphology. Specimens were coated with gold-palladium for 120 seconds using vacuum sputtering device (Cressington, 108 Sputter). To assess cell morphology, the following protocol was employed for preparing scaffolds:

1. A solution of 2.5% glutaraldehyde in 0.1 M PBS was prepared, and cells were fixed with this solution for 2.5 hours.

2. Following the removal of the fixation solution, a dehydration step was executed by introducing various concentrations of ethanol solutions to the scaffolds (35%, 50%, 70%, 80%, 90%, 95%, and 100%). In each concentration, cells were incubated for 10 minutes, except for 15 minutes in the case of 100% ethanol.

3. After ethanol removal, Hexamethyldisilane (HMDS) solutions with varying concentrations (50%, 60%, 70%, 80%, 90%, and 100%) were added and incubated for 10 minutes for each concentration. HMDS was chosen for its role as a drying agent, aiding in moisture removal from the sample. The critical point drying process involving HMDS proves especially advantageous for preserving cell structures, mitigating the detrimental effects associated with conventional drying methods. The 100% HMDS solution was left under the hood overnight with an open well-plate lid to facilitate HMDS evaporation. Following the drying process, samples were coated using the previous protocol.

3.5.3 Mechanical Properties Evaluation

Compression and tension tests were carried out for PCL-nHA scaffolds. Tests were done with MARK-10 (Mark-10 Corporation, USA) device with a 1 kN load cell as shown in Figure 15. Test setup used for tensile and compression testing using a) MARK-10 UTM machine with b) images during compression testing of scaffolds.. Compression tests were done at 2 mm/min and tensile tests were conducted at 1 mm/min (J. W. Kim et al., 2017a).

Figure 15. Test setup used for tensile and compression testing using a) MARK-10 UTM machine with b) images during compression testing of scaffolds.

3.5.4 Contact Angle Measurement

The hydrophilicity assessment of the 3D scaffolds involved contact angle measurements conducted with the Attension Theta Lite Optical Tensiometer (Nanoscience, USA). A volume of 2.5 µL of distilled water was applied onto the thin film samples using the sessile drop method. To ensure accuracy, each set of measurements was repeated three times, enabling the calculation of the average contact angle for the scaffolds' surface.

3.5.5 Viscosity Analysis

The MCR 92 Rheometer (Anton Paar, Austria) was utilised to examine the viscosity of the PCL15HA10 solution at two distinct solution ages, namely 1 day and 13 days. This analysis aimed to elucidate the viscosity characteristics and solution behaviour under shear conditions. The experimental setup employed a parallel plate head with a 1 mm gap, and assessments were conducted through amplitude sweep tests and viscosity measurements.

3.5.6 Characterization of Nanoparticles

The morphology of gelatin nanoparticles was assessed using SEM (Zeiss Leo Supra VP 35 field emission). The specimens were created by depositing 10 µl of the rinsed nanoparticle solution onto the silicon wafer's surface and allowing it to air dry for a duration of 2 hours at ambient temperature. The surface of the wafer was spray-coated with gold/palladium under vacuum by using Denton sputtering machine for 40 seconds, three times prior to imaging.

Z-average size and polydispersity measurements of the nanoparticles were done three times for each specimen by dynamic light scattering (DLS), using a Zetasizer Nano-ZS (Malvern Instruments Ltd., UK).

3.6 In vitro Studies

MC3T3-E1 subclone 4 (ATCC CRL-2593) was used for cell culture studies. Alpha-MEM (Gibco) supplemented with 10% Fetal Bovine Serum (Pan Biotech) and 1% Penicillin-Streptomycin solution (Pan Biotech) was used as growth medium.

Scaffolds were sterilized by washing with sterile 1X DPBS and then placed in 70% ethanol for one hour. Then, ethanol was removed, and scaffolds washed with 1X DPBS twice for 15 minutes. After removing the DPBS, each side of the scaffold was subjected to UV light for one hour.

Sterilised scaffolds were seeded with 5200 cells/cm2 in 100 µl growth medium, and cultured for 2 hours in 37°C, in an incubator. The cell seeding was performed in a hydrophobic culture dish to ensure that the cells adhered to the scaffold rather than the dish itself. After 2 hours of culture, scaffolds are moved to the 24 well cell culture plate and 1 ml growth medium was added.

3.6.1 Cell Metabolic Activity Assessment

To assess the metabolic activity of the cells, MTS assay (CellTiter 96 Aqueous One Solution Cell Proliferation Assay, Promega) was used. The measurements were carried out on the 7th, 14th and 21st days. The medium was refreshed every other day. To summarize, the growth medium was discarded and replaced with an MTS solution of 120 µl, along with 600 µl of growth medium, in each well. The mixture was then incubated for 4 hours at 37 °C with a 5% CO_2 concentration. Following incubation, 200 µl of the solution was dispensed into a 96-well plate in triplicates. The absorbance of the samples was then assessed at a wavelength of 490 nm utilizing a plate reader (Infinite 200 Pro, Tecan).

3.6.2 Alkaline Phosphatase Activity Assessment

Cells were cultured on both uniform and FGSs for a duration of 21 days. For prompting osteogenic differentiation, the cells were exposed to an osteogenic medium supplemented with 10 µg/ml ascorbic acid (Sigma) and 3 mM β-Glycerophosphate (Sigma). This medium was introduced after the initial 3 days of culture. Alkaline phosphatase (ALP) activity assessments were conducted on days 7, 14, and 21.

Briefly, cellular lysates were derived using M-PER (Mammalian Protein Extraction Reagent, Thermo Scientific). A mixture of 2 µl of this lysate and 2 µl of the ALP assay kit's substrate (Alkaline Phosphatase, Diethanolamine Detection Kit, Sigma Aldrich) was incubated for 45 minutes, followed by absorbance readings at 405 nm.

The ALP activity was normalized by utilizing the Bradford assay to measure the total protein concentration of each sample.

3.6.3 Phalloidin and DAPI Staining

Phalloidin and DAPI staining were used to evaluate cell morphology. Briefly, cell cultured samples were treated with a 4% paraformaldehyde (PFA) solution and fixed for a duration of 30 minutes at ambient temperature. Following this, the specimens underwent treatment with a solution comprising 0.1% Triton X-100 in DPBS for a duration of 15 minutes at room temperature. This step was performed to enhance the cells' permeability. Subsequently, the samples were blocked with a 1% bovine serum albumin (BSA) solution in PBS for 45 minutes at room temperature. The samples were sliced using a microtome blade in order to examine the central section. The specimens were subsequently placed in a dark environment at room temperature for a duration of one hour, where they were treated with Phalloidin Alexa Fluor 546 (Invitrogen) that had been diluted to a concentration of 1:400 in DPBS. After the incubation period, the phalloidin solution was removed, and the specimens were rinsed with sterile 1X DPBS. Finally, the samples were placed on a confocal dish, and a drop of Fluoroshield with DAPI (diamidino-2-phenylindole) (Sigma) was added. After a 5-minute incubation in the dark, the samples were observed using a confocal microscope (Zeiss, LSM 710).

3.6.4 Release Studies

To examine the release profile of BMP-2 growth factor, an enzyme-linked immunosorbent assay (ELISA) targeting bone morphogenetic protein 2 (BMP-2; AFG Scientific, US) was conducted.

In the preliminary phase of the study, the scaffolds were directly loaded with BMP-2. To elaborate, 50 ng of BMP-2 was applied to both uniform and FGS scaffolds, and the scaffolds were then incubated for 2 hours at 37°C in an incubator. Following incubation, the scaffolds were moved to a 24-well plate, and then 1 ml of DPBS was introduced, followed by a 5-minute agitation period. The resulting solution represented the fraction of BMP-2-loaded gelatin nanoparticles that remained unbound.

Subsequently, an additional 1 ml of DPBS was introduced, and specimens were collected from the scaffolds at various time intervals, specifically at 4, 12, 24, 48, 72, 160 and 336 hours. These collected samples were subjected to an ELISA assay for further analysis.

After completing the first phase of the study as described above, 50 ng/100 µl of BMP-2 loaded gelatin nanoparticles was introduced to both sterile uniform and functionally graded scaffolds, followed by a 2-hour incubation at 37°C within an incubator. Post-incubation, the scaffolds were moved to a 24-well plate, and 1 ml of DPBS was added, followed by a 5-minute agitation. The resulting solution represented the fraction of unbound BMP-2-loaded gelatin nanoparticles. Subsequently, an additional 1 ml of DPBS was added, and samples were collected from the scaffolds at various time points, specifically at 2, 4, 8, 12, 24, 48, and 72 hours. These collected samples were then subjected to ELISA assay for further analysis.

Chapter 4

Results and Discussion

The chapter presents findings from the in-depth characterization studies along with comprehensive discussions. Firstly, porosity analysis using micro-CT is presented. Subsequently, mechanical properties are assessed through UTM test results. The viscosity of the PCL-HA solution is evaluated using a rheometer, and the findings are presented herein. Contact angle measurements were conducted for both PCL-HA scaffolds and gelatin nanoparticle-loaded PCL-HA scaffolds. In vitro tests were performed for both types of scaffolds— PCL-HA and gelatin nanoparticle-loaded PCL-HA scaffolds. These tests included the MTS assay for cell viability assessment, ALP assay for alkaline phosphatase activity measurement, phalloidin and DAPI for cell morphology observation, and ELISA assay for BMP-2 release studies.

4.1 Morphological characterization with micro-CT

Figure 16. Computed tomography (CT) scans of three-dimensional (3D) uniform and FGS scaffolds captured from top and side view. illustrates top and side views of the reconstructed 3D images of sample uniform and FGS scaffolds using micro-CT. To carry out the examination, 51 segments of the volumetric region of interest (VOI) were pinpointed from three separate areas, each possessing its individual distinct ROI. When compared with the desired morphology, overall, it is noted that the desired strut and macro-pore dimensions were achieved as apparent in top view image with slight deviations along the longitudinal direction as is apparent in the side view images. Overall, the desired macro-pore morphology was maintained but vertical struts and pored showed angular orientation deviations depending on the used printing velocity and pressure.

Figure 16. Computed tomography (CT) scans of three-dimensional (3D) uniform and FGS scaffolds captured from top and side view.

Table 2. Measured and theoretical porosity analysis results

	Uniform Structure	FGS Structure
Stl File Structure Size	10.5 x 10.5 x 3.0 mm	14.08 x 14.08 x 3.59 mm
Theoretical Macroporosity	61.8 %	62.8 %
Measured Porosity	79.9 %	73.0 %
Difference Between Measured Porosity vs. Theoretical Porosity	22.65 %	13.97 %

4.2 Mechanical Properties Evaluation

To assess the mechanical characteristics of the FGS and uniform scaffolds, we conducted tensile and compression tests. Stress-strain curves were generated to illustrate the behaviour of the scaffolds subjected to tension and compression forces. As shown in Figure 17 , the stress values for the FGS scaffolds were lower than those for the uniform scaffold. The stress-strain curves suggest a comparable mechanical consistency between the uniform and functionally graded scaffolds, highlighting the effectiveness of the fabrication process. It is conceivable that the uniform scaffold, with its homogeneous material distribution, exhibits higher stress values due to a more concentrated load-

bearing capacity. Conversely, the FGS scaffolds' lower stress levels can be attributed to its gradient structure, which influences the distribution of compressive forces. Although the uniform scaffold demonstrates superior stress resistance, the functionally graded scaffold may offer advantages in terms of flexibility or adaptability, as indicated by its lower stress values. It is noted that the compression tests are carried out with compression applied along the thickness of the scaffolds as shown in the side view while tensile tests are carried out w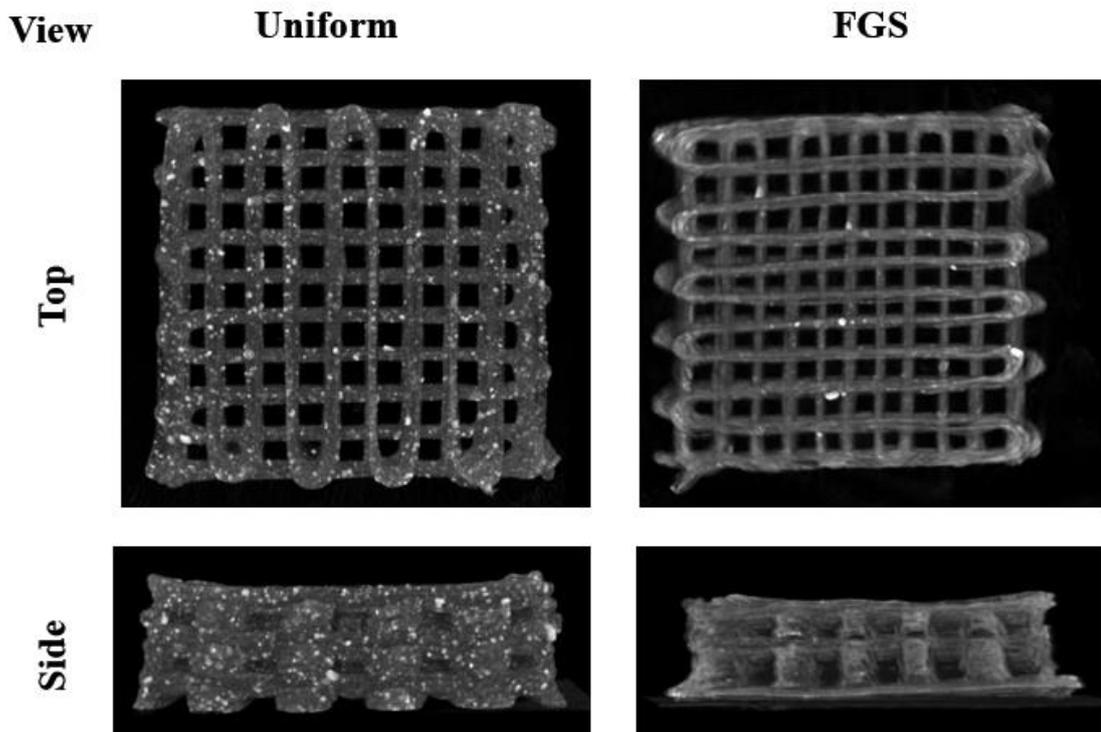ith tension applied along the x or y dimension of the top view as shown in Figure 16. Computed tomography (CT) scans of three-dimensional (3D) uniform and FGS scaffolds captured from top and side view.. Since the produced load bearing surface area and dimensions, despite similar porosities of FGS and uniform scaffolds are not the same, a one-to-one comparison is not possible especially for the compression test where the surface area is more than twice the area for the FGS vs. uniform scaffolds. More thorough assessment with possibly comparable surface area, dimensions and porosities are needed.
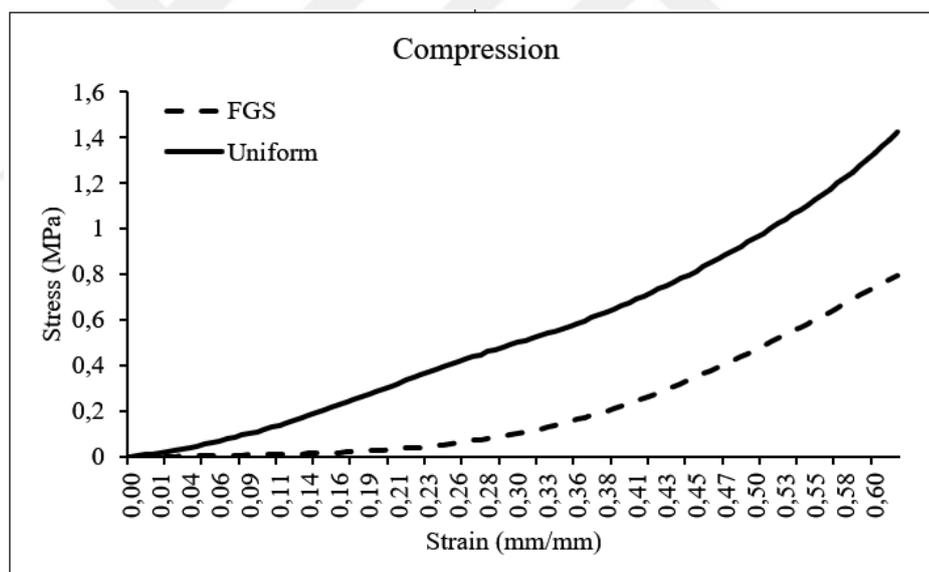

Figure 17. Stress vs. strain data obtained using compression test for FGS vs. uniform scaffolds (n=3).
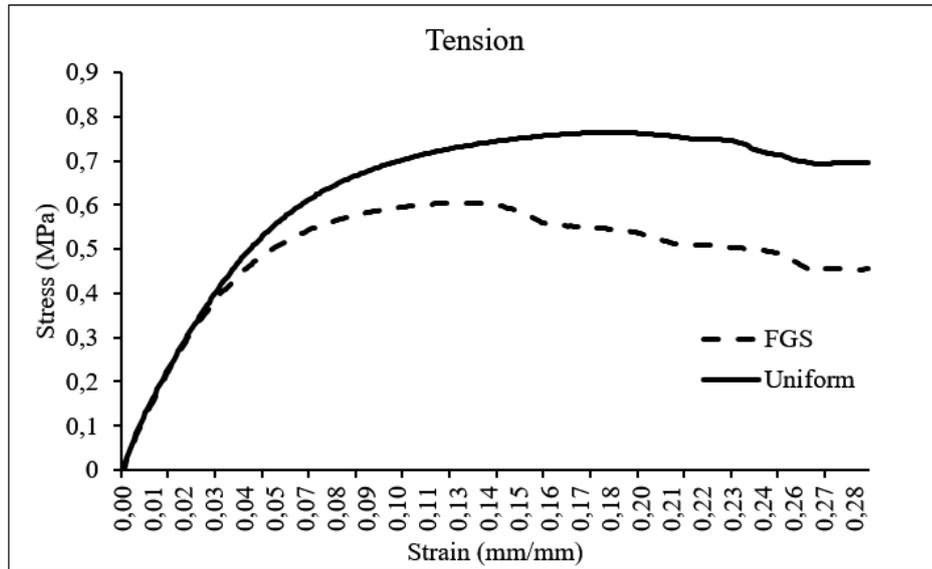
Figure 18. Stress vs. strain data obtained using tension test for FGS vs. uniform scaffolds (n=3).

Table 3. Compressive and Tensile Modulus of FGS and Uniform scaffolds

	Tensile Moduli (MPa)	Compressive Moduli (MPa)
FGS	$11,53 \pm 2,42$	$2,17 \pm 0,082$
Uniform	$10,41 \pm 2,98$	$2,67 \pm 0,14$

4.3 Contact Angle Measurement

The results of contact angle measurements on PCL15HA10 film specimens loaded with GNP are presented in Table 4 and Figure 19**Table 4.** Contact angle values for gelatin nanoparticle loaded scaffolds and unloaded scaffolds.. The hydrophilic properties of these scaffolds are crucial in influencing cell adhesion and growth. The incorporation of gelatin nanoparticles into the scaffolds resulted in a significant reduction in the contact angle, suggesting that the presence of gelatin nanoparticles greatly enhanced the hydrophilicity of the scaffolds. Prior investigations have provided detailed insights into the influence of gelatin nanoparticles, serving as a hydrophilic polymer, on decreasing the contact angle exhibited by synthetic hydrophobic polymers (Kozehkonan et al., 2019; Li et al., 2014; Shahrezaee et al., 2018).

Table 4. Contact angle values for gelatin nanoparticle loaded scaffolds and unloaded scaffolds.

PCL15HA10 without GNP	PCL15HA10 with GNP
85.9 ° ± 2.9	25.7 ° ± 4.4

PCL15HA10   PCL15HA10 with GNP
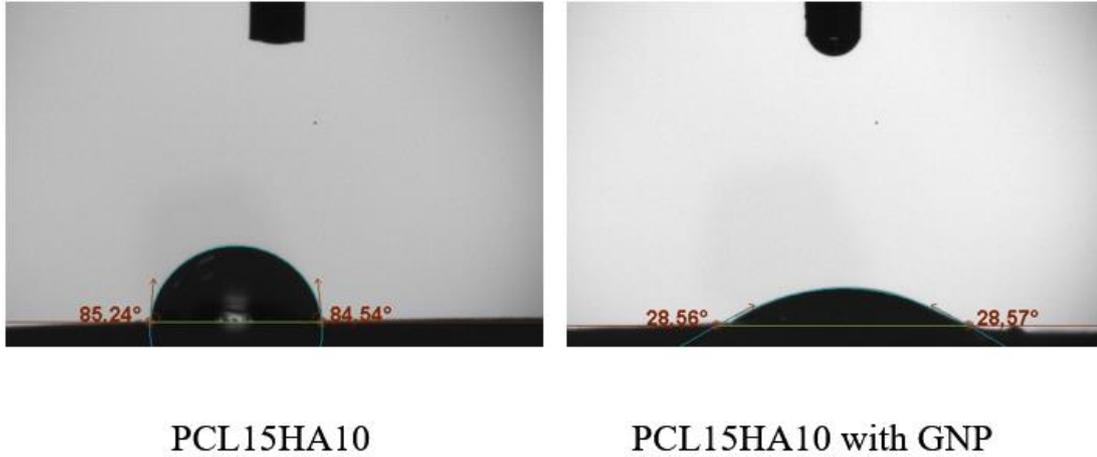
Figure 19. Contact angle measurements of gelatin nanoparticle loaded film scaffolds and unloaded film scaffolds, n=3.

4.5 Viscosity Analysis

The viscosity-shear rate outcomes for the PCL-HA with 15% PCL and 10% nHA solution used for producing uniform and FGSs were assessed and are illustrated in Figure 20. The viscosity vs. shear rate graph depicts a dynamic rheological behaviour of the material within a range of shear rates. The material undergoes a substantial decrease in viscosity as the shear rate increases. This observed trend signifies a shear-thinning behaviour. The significant drop in viscosity suggests that the material is responsive to varying shear conditions, which can have practical implications in applications requiring flow under stress. The shear-thinning nature, evident in the graph, may be advantageous for processes involving injection or flow, making the material more adaptable to dynamic conditions. Importantly, the observed shear-thinning behaviour indicates non-Newtonian fluid characteristics, distinguishing it from fluids with constant viscosity, thus aligning with the complexities of non-Newtonian rheology. The measured viscosity is consistently in the range with earlier measurements (Bilgili et al., 2024).
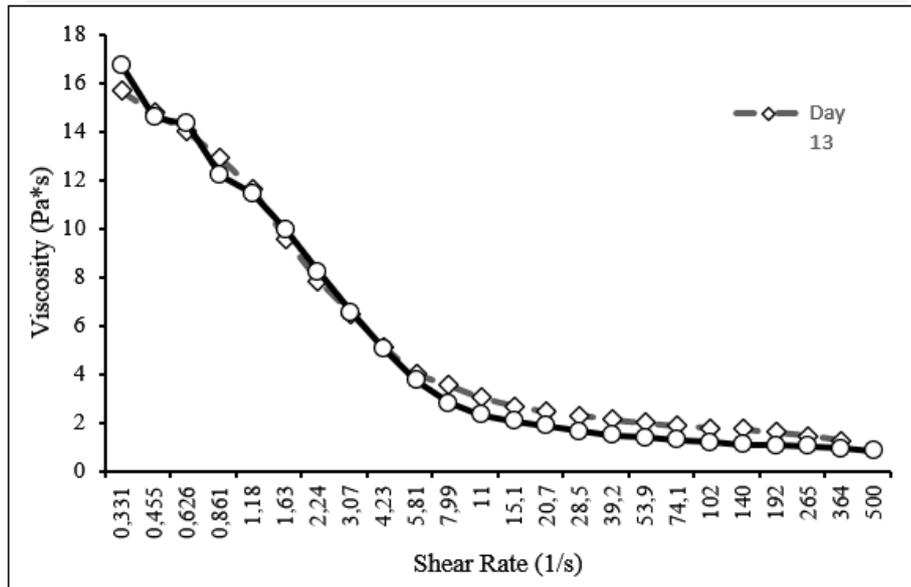
Figure 20. Viscosity versus shear rate measurements for PCL-HA solution carried out at day 1 and day 13 using Anton Paar MCR 92 rheometer device.
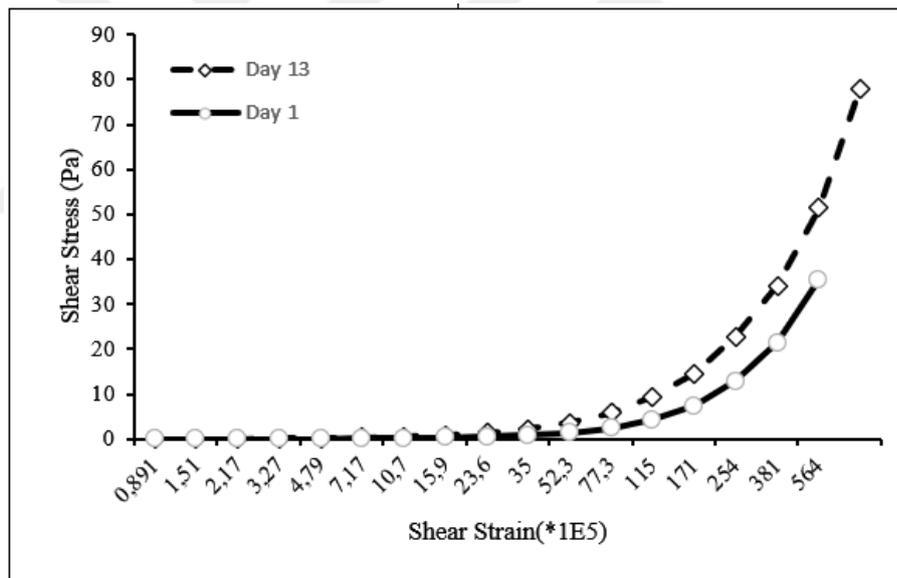
Figure 21. Shear Stress versus shear strain measurements.

4.6 Characterization of Nanoparticles

Gelatin nanoparticles in aqueous solutions were characterised using dynamic light scattering to determine their average size or diameter. The gelatin nanoparticles were found to have a hydrodynamic diameter of 144.4 ± 2.7 nm upon measurement, demonstrating a monodisperse size (polydispersity index = 0.01). Scanning electron microscopy analysis confirmed the gelatin nanoparticles exhibited a round shape (Figure

23. SEM images of the produced GNPs, a) with 50K magnification and b)100K magnification.). Visual examination of the nanoparticles indicated that the majority is within the size range of 100-150 nm, consistent with the dynamic light scattering results (Figure 22. DLS analysis of produced gelatin nanoparticles obtained from Zetasizer Nano-ZS, n=3.). Interestingly, the mean diameter obtained from scanning electron microscopy (~104 nm) was found to be smaller than the hydrodynamic diameter. The variation in measurements can be ascribed to the distinction in the methodologies employed: SEM quantifies the diameter of the particle in its dry state, while DLS considers the hydrodynamic diameter, incorporating the influence of hydrated layers on the particle surface.

BMP-2 loading to gelatin nanoparticles was found to be 85,79 %. The measurements were carried out as discussed in section 3.4.

Figure 22. DLS analysis of produced gelatin nanoparticles obtained from Zetasizer Nano-ZS, n=3.

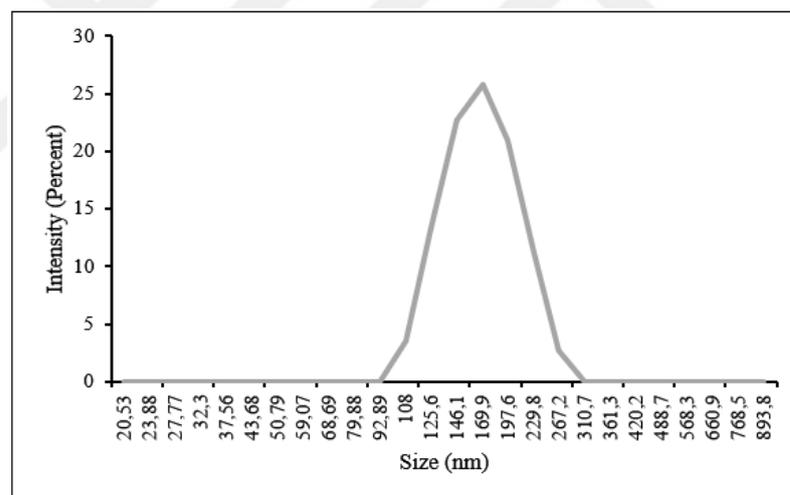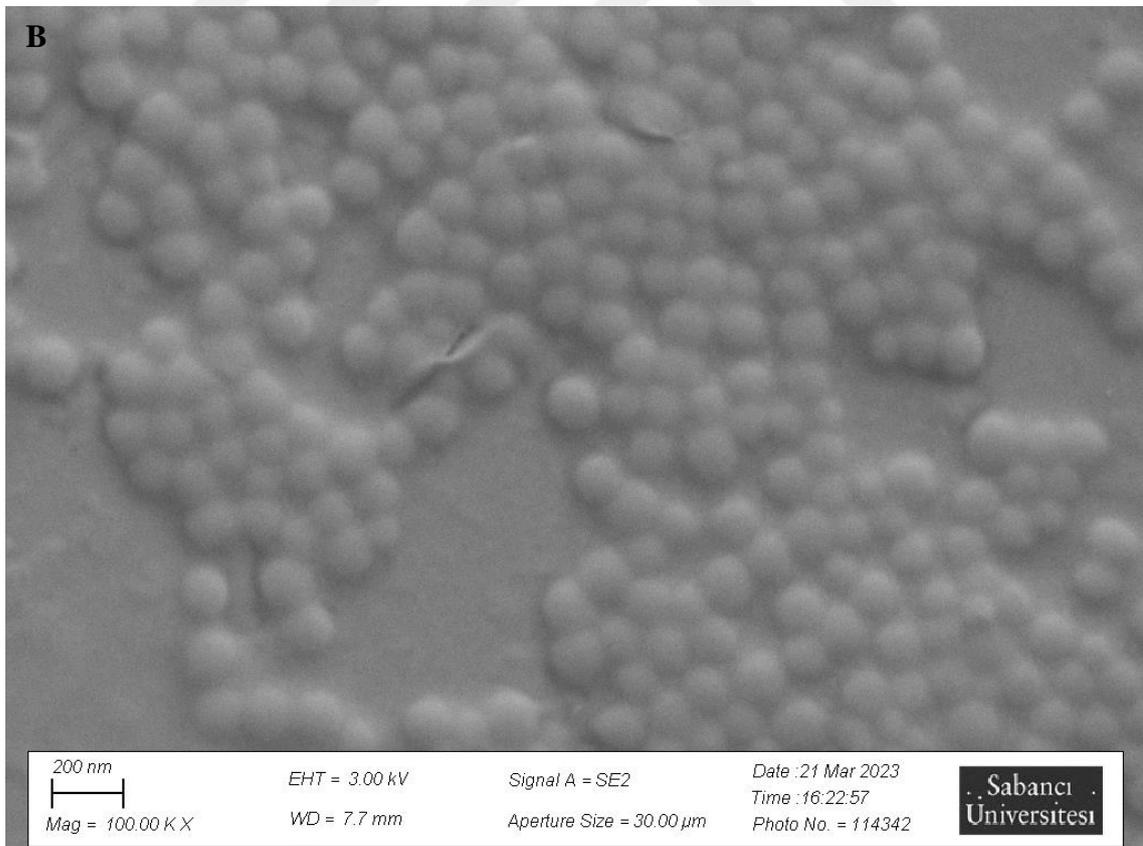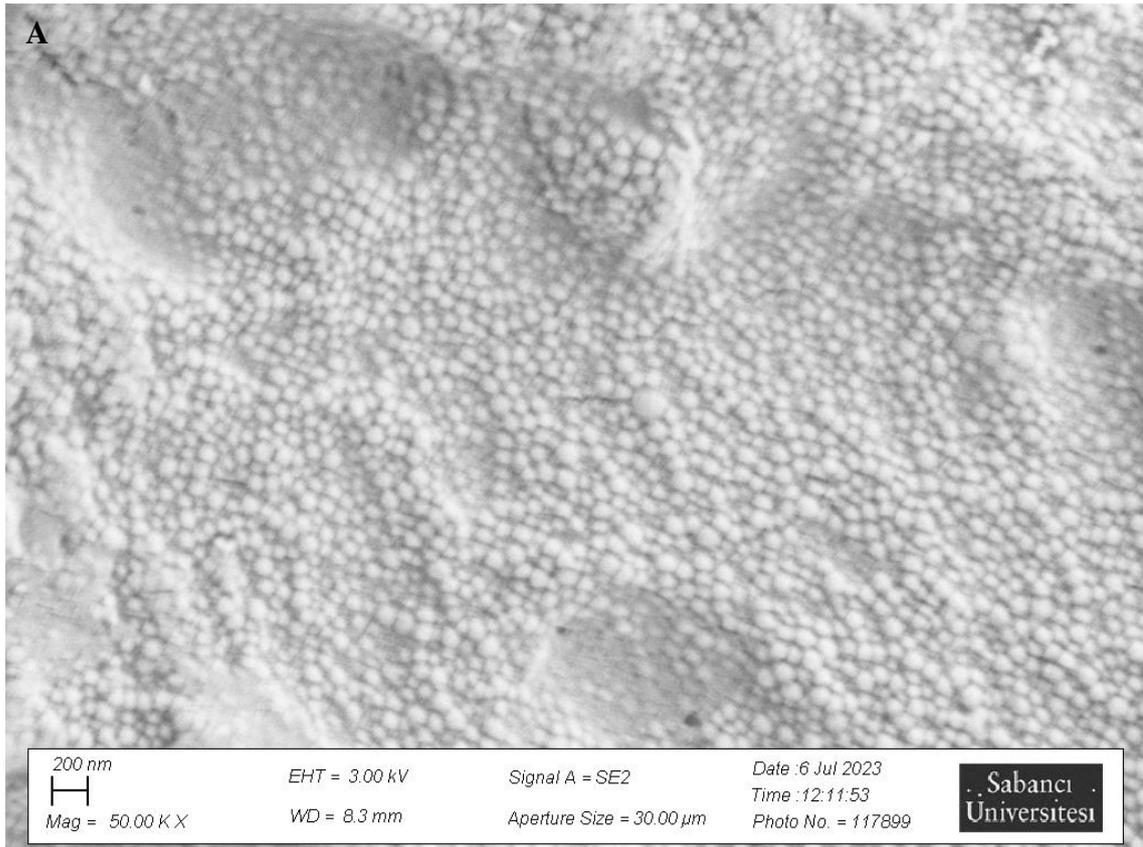**Figure 23.** SEM images of the produced GNPs, a) with 50K magnification and b)100K magnification.

4.8 Cell Metabolic Activity Assessment

Two distinct geometries were used to construct scaffolds made of 15% PCL and 10% nHA, on which MC3T3-E1 cells were cultured. The MTS assay results for bone tissue scaffolds with uniform and FGS reveal notable differences in cell viability and proliferation dynamics as seen in Figure 24. Percentage viability results of MTS assay for BMP-2 encapsulated GNP loaded FGS and uniform scaffolds, n=3. While both scaffold types support cell viability over the experimental period, the uniform scaffold consistently exhibits higher cell viability percentages compared to the FGS scaffold at each time point. Moreover, the uniform scaffold demonstrates a more rapid increase in cell viability, indicating a higher proliferation rate. However, both scaffold types eventually achieve high levels of cell viability by day 21, suggesting their potential for supporting cell growth. While the FGS scaffold initially shows lower cell viability compared to the uniform scaffold, it still demonstrates a significant improvement in cell viability over time. This suggests that despite the initial difference, the functionally graded structure scaffold is capable of supporting cell proliferation and achieving high cell viability by the end of the experimental period.
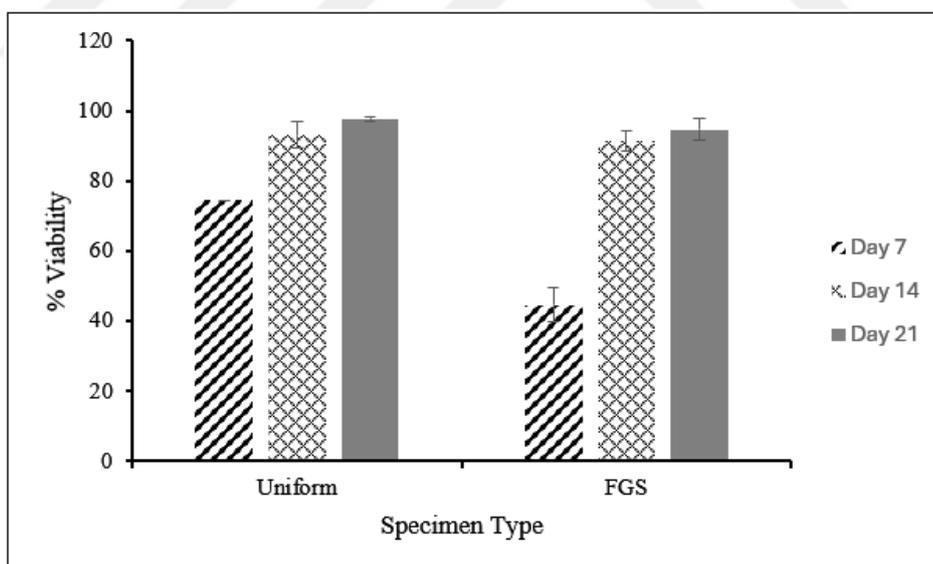
Figure 24. Percentage viability results of MTS assay for BMP-2 encapsulated GNP loaded FGS and uniform scaffolds, n=3

4.9 Alkaline Phosphatase Activity Assessment

The ALP activity was assessed for both the FGS and uniform scaffolds, in the presence of BMP-2 encapsulated gelatin nanoparticles. Figure 25 shows the graph obtained from ALP assay. Initially, on day 7, both scaffold types and the control cells exhibited ALP activity, indicating early osteogenic differentiation. However, from day 7 to day 14, there was a decrease in ALP activity for all samples, including both scaffold types and the control cells. This unexpected decrease may reflect a transition phase in osteogenic differentiation or changes in cellular behaviour. By day 21, ALP activity continued to decrease for all samples, contrary to the expected trend of increasing osteogenic differentiation over time. This unexpected decrease suggests potential limitations or challenges within the experimental setup or cellular environment that impact osteogenic differentiation. Further investigation is warranted to identify and address the factors contributing to the observed decrease in ALP activity and possible experimental errors. It is noted that the BSA standard was conducted using 1mg/ml.
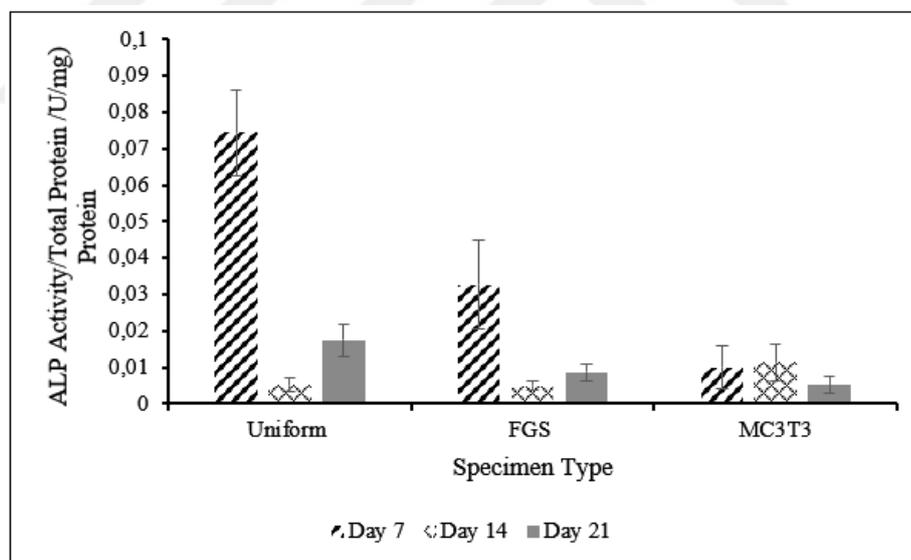
Figure 25. ALP activity results of MC3T3 cells on uniform and FGS scaffolds, normalized with Bradford assay results, n=3

4.10 Phalloidin and DAPI Staining

Cells on the scaffolds were imaged with confocal microscopy at 7, 14, and 21 days of culture to assess the distribution and morphology of cells on both uniform and FGS scaffolds. The results, as seen in the Figure 26 and Figure 27, indicated that each scaffold

proficiently supported cell growth within the tissue scaffold. Over the course of the 21-day culture period, there was a continual and consistent enhancement in both cell proliferation and distribution on both types of scaffolds, a trend further validated by the cell proliferation assay.
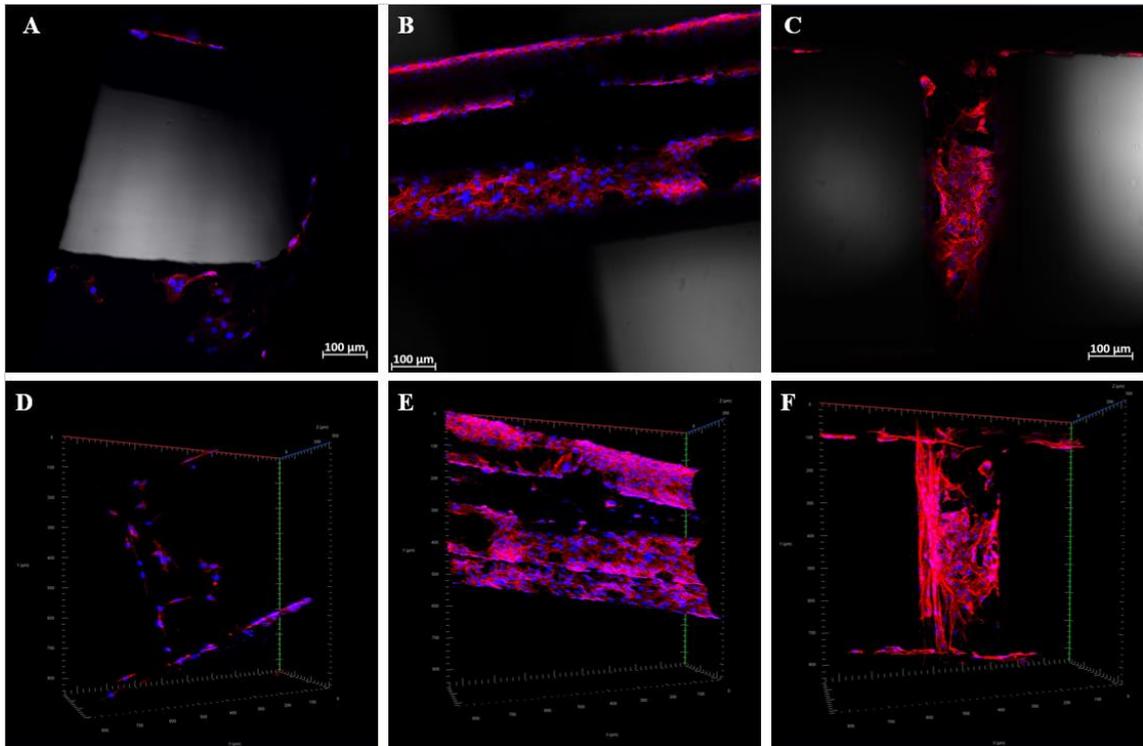
Figure 26. Confocal images using DAPI (blue) and Phalloidin (red) staining on Uniform scaffolds, Morphologies Day 7, day 14, day 21 (A, B, C, respectively), Distributions Day 7, day 14, day 21 (D, E, F, respectively)
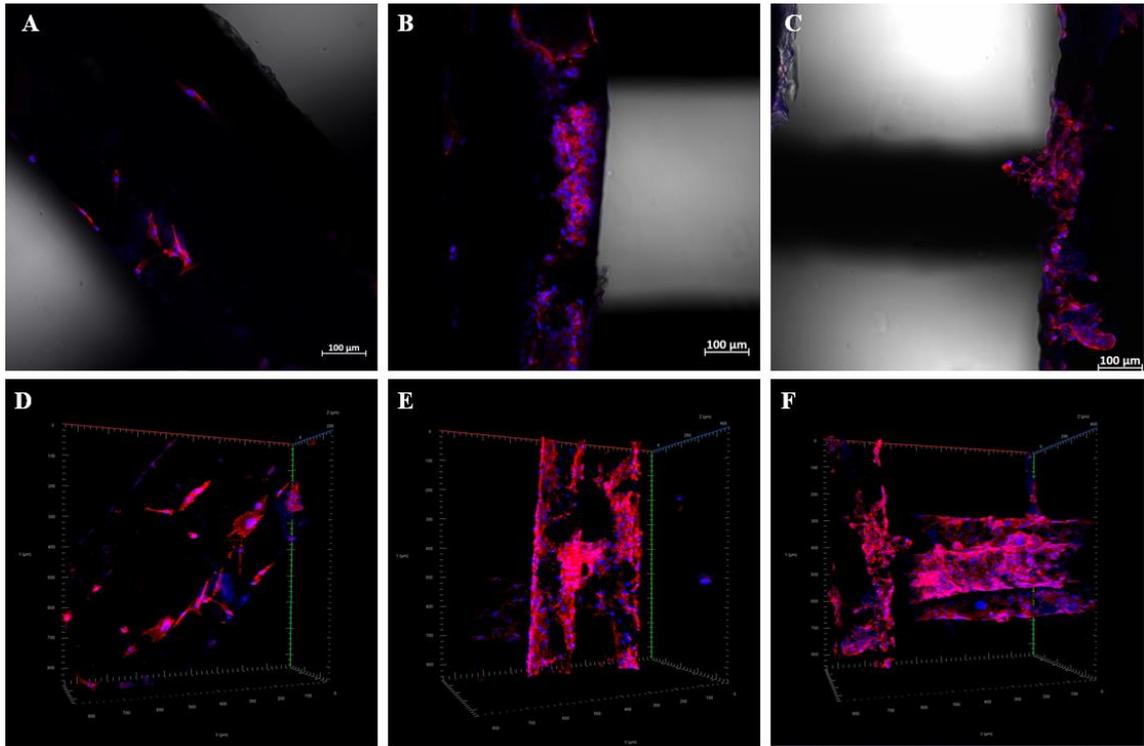
Figure 27. Confocal images using DAPI (blue)and Phalloidin (red) staining on FGS scaffolds, Morphologies Day 7, day 14, day 21 (A, B, C, respectively), Distributions Day 7, day 14, day 21 (D, E, F, respectively)

4.11 Cell Morphology Analysis with SEM

To acquire morphological information on cell attachment to 3D PCL-HA scaffolds featuring distinct geometries, scanning electron microscopy (SEM) was utilised for imaging cells on the 7th, 14th, and 21st days. The findings indicate that cells displayed favourable attachment on the surfaces of both the uniform and FGS scaffolds (Figure 28). In consistency with the confocal images, cells demonstrated good attachment on the surface of scaffolds continuously with more dense cell occupation for the uniform scaffolds than for FGS scaffolds on day 7. On day 14, it was observed that the cells occupied the majority of scaffold strut surfaces with some bridging over the struts for FGS scaffolds. On day 21, the cell morphology displayed clear borders for uniform scaffolds when compared with FGS scaffolds. Overall, the scaffold surface, rather than the pore regions, was covered by interconnected cells in both type of scaffolds.
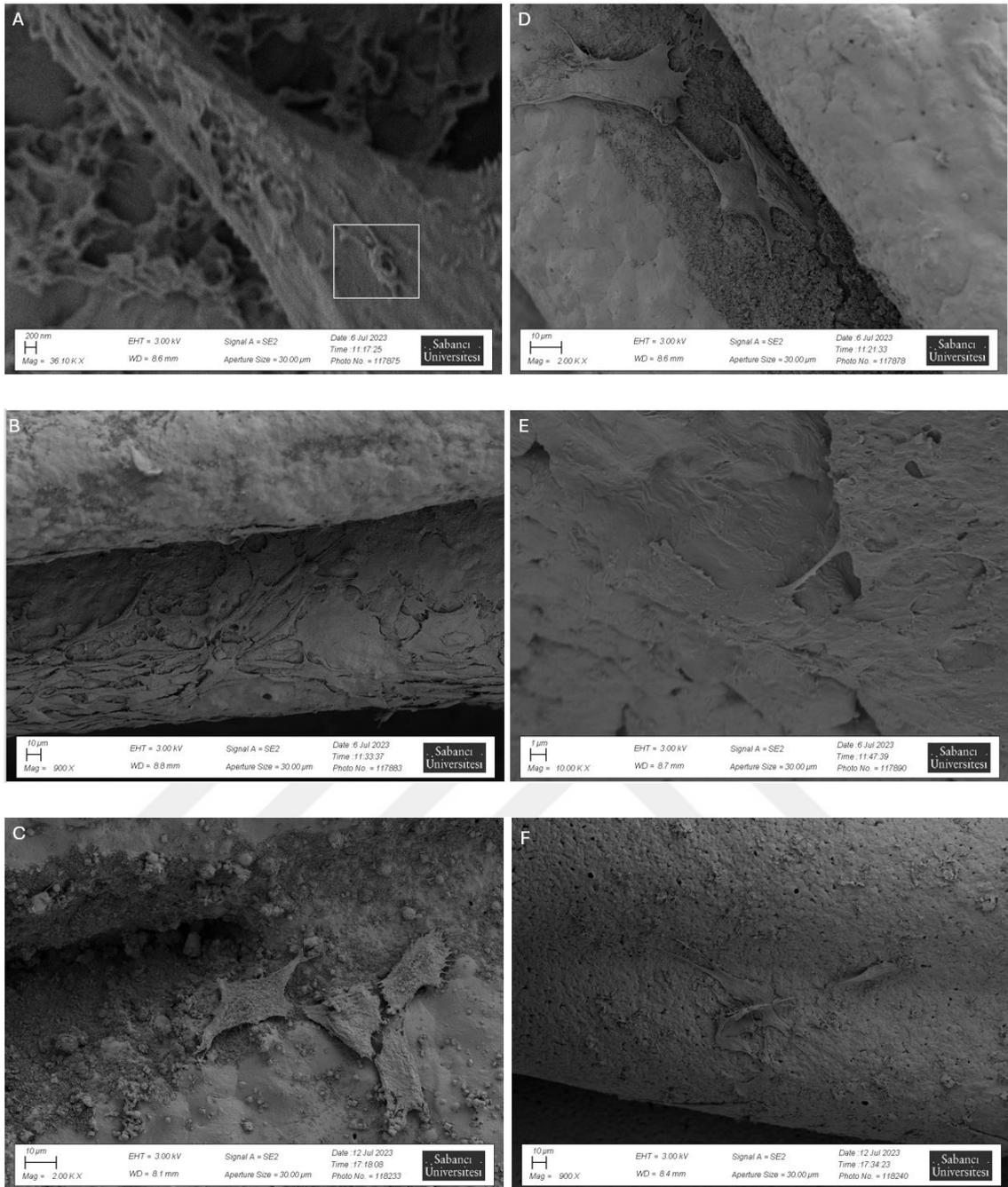
Figure 28. SEM images showing cell morphologies on uniform (A, B, C) and FGSs (D, E, F) during a culture period of 7 (A, D), 14 (B, E), and 21 (C, F) days.

4.12 Release Studies

Figure 29 shows the release pattern of BMP-2 loaded uniform and FGS scaffolds that do not contain any GNP. Based on the trend of the release curve, an increase of release behaviour is observed in the first hours, and a stable profile is observed thereafter. However, regarding the values of the released concentration when compared with the initially loaded BMP-2 concentration of 50 ng/100 μl, it can be deduced that actually almost no BMP-2 was released due to the very low release percentage value of 500 pg/50 ng. It may be argued that the BMP-2 growth factors are trapped within the scaffold or this seemingly unexpected result may be due to problems in the BMP-2 ELISA kit or other experimental uncertainties which prompts for further investigation possibly with a control group of gelatin nanoparticles and repeated tests investigating the effect of the BMP-2 loading and the release experiments.

Figure 30 illustrates the release pattern of BMP-2-GNP in a PBS buffer solution. In both scaffold configurations, a rapid release was observed within the initial 8 hours. Unlike in the case where GNPs were not present, the concentration values call for a significant release behaviour in case where BMP-2 was encapsulated within gelatin nanoparticles. Between the 12th and 72nd hours, the release of BMP-2 exhibited a more consistent increase. Notably, release from FGS scaffolds were relatively higher than uniform scaffolds. Due to the structural characteristics of the FGS scaffolds, with larger pores on the outer surface area regions while smaller pores occupying the central region, the measured release profile from the FGSs, compared to uniform scaffolds, agrees with the expected release pattern.

The total release of BMP-2 over a 72-hour immersion period was calculated as 49,267 pg/ml and 54,250 pg/ml for uniform and FGS scaffolds, respectively. The initially loaded amount of BMP-2 was 50 ng/100 μl, and this loaded BMP-2 was released from both scaffolds within the 3-day period. Discrepancies between the loaded and measured BMP-2 levels could be attributed to the ELISA kit. An issue with the expiration date of the ELISA kit may be a contributing factor to this discrepancy. Overall, it can be still deduced that the observed continuous release behaviour of BMP-2 suggests that gelatin NPs are effective in delivering growth factors with an initial burst release in the first 24 hours followed by a more sustained release thereafter. However, it would be necessary to carry out repeated readings.
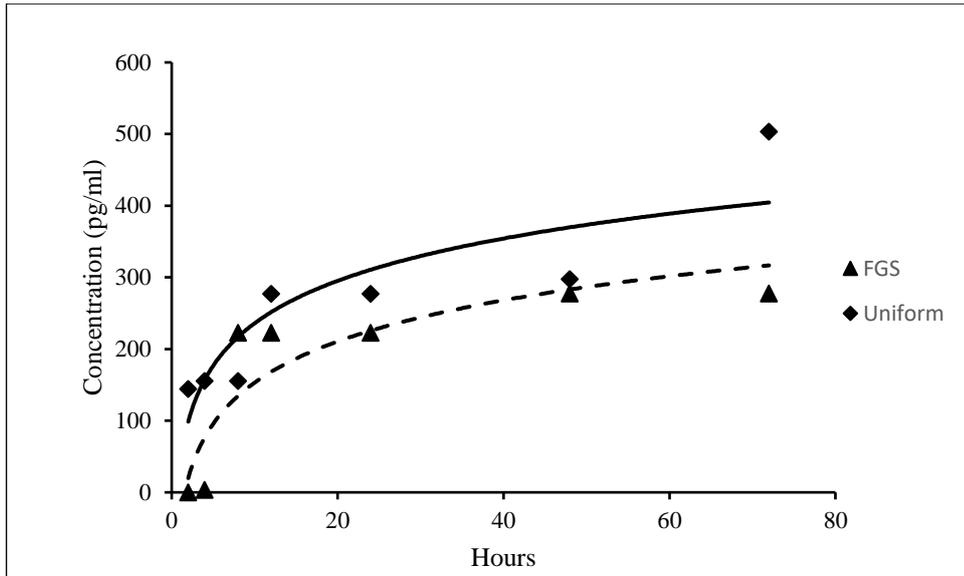
Figure 29. BMP-2 cumulative release results obtained for uniform and FGS scaffolds with no GP loading using ELISA, n=1
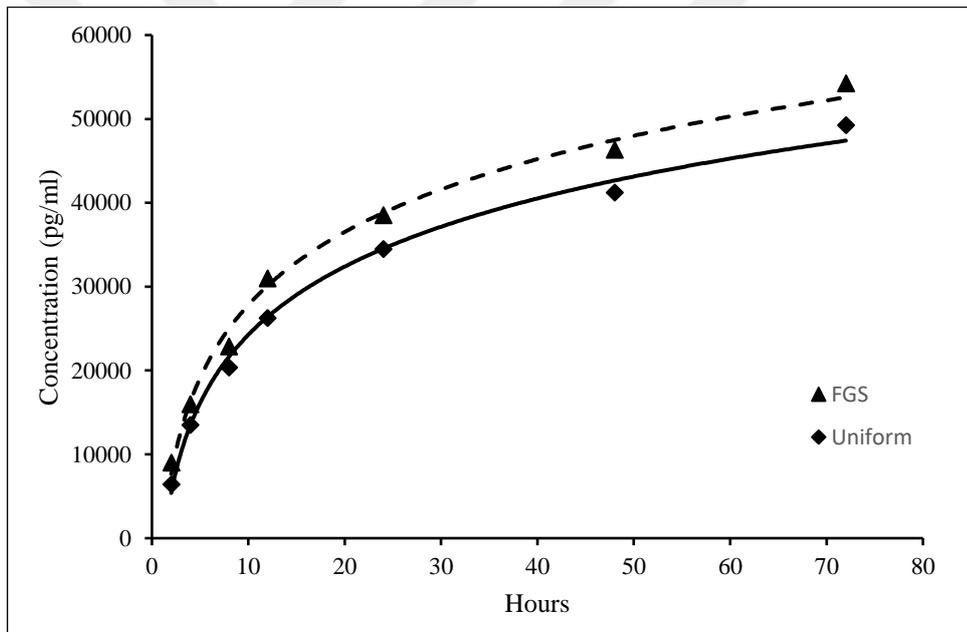
Figure 30. BMP-2-GNP cumulative release results obtained for uniform and FGS scaffolds with ELISA, n=1

Chapter 5

Conclusions and Future Work

5.1 Conclusions

This thesis focused on the analysis of FGS and uniform scaffolds while examining the impact and release kinetics of BMP-2 loaded GNPs. The scaffolds analysed in this thesis were fabricated using a combination of the earlier proposed Non-Solvent-Induced Phase Separation (NIPS) method and 3D printing and therefore displayed multi-scale porosity and spatially varying macropores mimicking natural bone tissue. Gelatin nanoparticles were created through a two-step desolvation method, and BMP-2 was encapsulated into these nanoparticles using a diffusion method. The incorporation of BMP-2 encapsulated gelatin nanoparticles into PCL-HA scaffolds of uniform and FGSs was achieved through adsorption. In particular, this study investigated the effect of morphology and BMP-2-gelatin nanoparticle loading on biological and release performance of uniform and functionally graded scaffolds.

To study these effects, a thorough investigation of scaffolds made of Polycaprolactone (PCL) and Nanohydroxyapatite (HA) featuring macro-pore gradients in multiple directions was conducted. Furthermore, the incorporation of BMP-2 loaded GNPs into both uniform and FGSs produced through the NIPS process integrated to 3D printing was presented, hence delivering scaffolds with multi-scale porosity. Using these scaffolds, our research presented an examination of the mechanical, biological and release performance by comparing PCL-HA uniform scaffolds with FGS scaffolds containing BMP-2 loaded gelatin nanoparticles. Experimental characterizations are carried out via mechanical UTM testing, imaging via micro-CT and scanning electron microscope (SEM), in-vitro testing including phalloidin and DAPI staining, alkaline phosphatase (ALP) activity and ELISA testing as well as confocal imaging.

The fabrication of both functionally graded and uniform 3D bone scaffolds have been accomplished successfully, and characterised both in vitro and mechanically. The resulting 3D scaffolds were thoroughly examined through micro-CT analysis, SEM, UTM analysis, and contact angle analysis. Furthermore, the gelatin nanoparticles that were produced underwent investigation using SEM imaging and DLS.

The micro-CT examination revealed that the porosity percentages for the uniform and FGS scaffolds were 79.9% and 73.0%, respectively. There were deviations both in dimensions and porosity which when considering the challenges faced in optimization of the printing conditions were deemed to be in the acceptable range. Using a UTM testing machine, the compressive modulus of uniform scaffolds was measured at 2.67 ± 0.14 MPa, while the tensile modulus was determined to be 10.41 ± 2.98 MPa. For FGS scaffolds, the compressive moduli were found to be 2.17 ± 0.082, and the tensile moduli were determined to be 11.53 ± 2.42 MPa. When considering differences in the overall cross-sections despite similar porosities, although not one-to-one comparable, both morphologies seemed to display suitable load bearing abilities and consistent results with literature. Contact angle results revealed values of $85.9° \pm 2.9$ for PCL-HA film scaffolds and $25.7° \pm 4.4$ for GNP-loaded PCL-HA film scaffolds with increased hydrophilic surface as expected with the incorporation of gelatin nanoparticles. Gelatin nanoparticle sizes were measured at 144.4 ± 2.7 nm, with a 0.01 PDI index using DLS measurements, and these measurements were confirmed through SEM imaging indicating repeatable manufacturing of GNPs around 150 nm suitable for BMP-2 encapsulation.

The in vitro assessments of scaffolds, whether featuring uniform porosity or varying porosity through non-uniform structures with gradient size porosity, revealed robust cell viability over a 21-day period with uniform scaffolds displaying comparatively increased cell viability when compared with FGS counterpart especially in the early 7 day and 14-day period. Regarding ALP activity measurements, from day 7 to day 14, there was a decrease in ALP activity for all samples, including both scaffold types and the control cells. This unexpected decrease may reflect a transition phase in osteogenic differentiation or changes in cellular behaviour. However, by day 21, ALP activity continued to decrease for all samples, contrary to the expected trend of increasing osteogenic differentiation over time. This unexpected decrease suggests potential limitations or challenges within the experimental setup or cellular environment that impact osteogenic differentiation. Further investigation is warranted to identify and address the factors contributing to the observed decrease in ALP activity and possible

experimental errors. Regarding phalloidin and DAPI staining measurements via confocal images, over the course of the 21-day culture period, there was a continual and consistent enhancement in both cell proliferation and distribution on both types of scaffolds, a trend further validated by the cell proliferation assay. Based on SEM imaging, consistent with confocal images, cells demonstrated good attachment on the surface of scaffolds continuously with more dense cell occupation for the uniform scaffolds than for FGS scaffolds on day 7. On day 14, it was observed that the cells occupied the majority of scaffold strut surfaces with some bridging over the struts for FGS scaffolds. On day 21, the cell morphology displayed clear borders for uniform scaffolds when compared with FGS scaffolds. Overall, the scaffold surface, rather than the pore regions, was covered by interconnected cells in both type of scaffolds. Finally, based on the very low released BMP-2 concentration values from scaffolds not adsorbed with GNPs, it may be argued that the BMP-2 growth factors are trapped within the scaffold or this seemingly unexpected result may be due to problems in the BMP-2 ELISA kit or other experimental uncertainties which prompts for further investigation possibly with a control group of gelatin nanoparticles and repeated tests investigating the effect of the BMP-2 loading and the release experiments. Unlike in the case where GNPs were not present, the concentration values call for a significant release behaviour in case where BMP-2 was encapsulated within gelatin nanoparticles. More specifically, the total release of BMP-2 over a 72-hour immersion period was calculated as 49,267 pg/ml and 54,250 pg/ml for uniform and FGS scaffolds, respectively. The initially loaded amount of BMP-2 was 50 ng/100 μl, and this loaded BMP-2 was released from both scaffolds within the 3-day period. Discrepancies between the loaded and measured BMP-2 levels could be attributed to the ELISA kit. An issue with the expiration date of the ELISA kit may be a contributing factor to this discrepancy as well as uncertainties associated with the experiment where a BSA standard of 1 mg/ml was used instead of a desired lower concentration of 0.1 - 0.5 mg/ml. Overall, it can be still deduced that the observed continuous release behaviour of BMP-2 suggests that gelatin NPs are effective in delivering growth factors with an initial burst release in the first 24 hours followed by a more sustained release thereafter. However, it would be necessary to carry out repeated readings at validated BSA standards with possibly more samples.

The results of this study indicate that 3D bone scaffolds both uniform and FGS developed in this study have significant potential in promoting osteoregeneration as effective mediators. Also, both morphologies, when adsorbed with BMP-2 encapsulated GNPs

produced via the two step desolvation method allow for a sustained release of growth factors. Specific differences related to their mechanical strength and comparative regeneration potential as well as release performances call for more thorough and repeated tests.

5.2 Future Work

In future research related to this thesis, there is an opportunity to further investigate cell viability, mineralization activity, and release kinetics. This could involve a more detailed examination of involved morphological parameters as well as manufacturing uncertainties, potentially under different experimental conditions or extending the study duration. In particular, additional repetitive set of ALP and phalloidin and DAPI staining and a repeated Elisa release test could prove to be very useful to be able to interpret the associated uncertainties. It is noted that the printing conditions were overall hard to be maintained and this gave rise to vertical alignment deviations that might have contributed to alterations of surface alignment which constitute areas for cell attachment and proliferation as well as pore size and alignment which play critical role in cell behaviour. Extending the focus from the current thesis, an alternative and novel approach could be pursued by exploring alternative blending methods, such as incorporating gelatin nanoparticles into the PCL-HA solution using different techniques. Additionally, to enhance the regenerative potential of the scaffolds, a promising avenue for future exploration is the integration of a second growth factor, such as Vascular Endothelial Growth Factor (VEGF). This strategic incorporation aims to stimulate angiogenesis, thus further contributing to the comprehensive tissue regeneration process. These proposed avenues for future work hold the potential to deepen our understanding and refine the design of biomimetic scaffolds, paving the way for more advanced applications in tissue engineering.

Bibliography

Abbasi, N., Hamlet, S., Love, R. M., & Nguyen, N. T. (2020). Porous scaffolds for bone regeneration. *Journal of Science: Advanced Materials and Devices*, *5*(1), 1–9. https://doi.org/10.1016/J.JSAMD.2020.01.007

Al-Himdani, S., Jessop, Z. M., Al-Sabah, A., Combellack, E., Ibrahim, A., Doak, S. H., Hart, A. M., Archer, C. W., Thornton, C. A., & Whitaker, I. S. (2017). Tissue-Engineered Solutions in Plastic and Reconstructive Surgery: Principles and Practice. *Frontiers in Surgery*, *4*. https://doi.org/10.3389/FSURG.2017.00004

Ashammakhi, N., Ghavaminejad, A., Tutar, R., Fricker, A., Roy, I., Chatzistavrou, X., Hoque Apu, E., Nguyen, K. L., Ahsan, T., Pountos, I., & Caterson, E. J. (2022). Highlights on Advancing Frontiers in Tissue Engineering. *Tissue Engineering - Part B: Reviews*, *28*(3), 633–664. https://doi.org/10.1089/TEN.TEB.2021.0012/ASSET/IMAGES/LARGE/TEN.TEB.2021.0012_FIGURE6.JPEG

Awad, H. A., O'Keefe, R. J., Lee, C. H., & Mao, J. J. (2014). Bone Tissue Engineering: Clinical Challenges and Emergent Advances in Orthopedic and Craniofacial Surgery. *Principles of Tissue Engineering: Fourth Edition*, 1733–1743. https://doi.org/10.1016/B978-0-12-398358-9.00083-5

Aydin, M. S., Sahin, M., Dogan, Z., & Kiziltas, G. (2023). Microstructural Characterization of PCL-HA Bone Scaffolds Based on Nonsolvent-Induced Phase Separation. *ACS Omega*. https://doi.org/10.1021/ACSOMEGA.3C05616/ASSET/IMAGES/LARGE/AO3C05616_0005.JPEG

Bahraminasab, M. (2020). Challenges on optimization of 3D-printed bone scaffolds. *BioMedical Engineering Online*, *19*(1), 1–33. https://doi.org/10.1186/S12938-020-00810-2/FIGURES/8

Bilgili, H. K., Aydin, M. S., Sahin, M., Sahin, S., Cetinel, S., & Kiziltas, G. (2024). Printed Functionally Graded PCL-HA Scaffolds with Multi-Scale Porosity. *Under Review in ACS Biomaterials Science and Engineering Journal*.

Buer Boyetey, M.-J., Torgbo, S., & Sukyai, P. (2023). Bio-scaffold for bone tissue engineering with focus on bacterial cellulose, biological materials for hydroxyapatite synthesis and growth factors. *European Polymer Journal*, *194*, 112168. https://doi.org/10.1016/J.EURPOLYMJ.2023.112168

Caballero Aguilar, L. M., Silva, S. M., & Moulton, S. E. (2019). Growth factor delivery: Defining the next generation platforms for tissue engineering. *Journal of Controlled Release*, *306*, 40–58. https://doi.org/10.1016/J.JCONREL.2019.05.028

Chandra, P. K., Soker, S., & Atala, A. (2020). Tissue engineering: Current status and future perspectives. *Principles of Tissue Engineering*, 1–35. https://doi.org/10.1016/B978-0-12-818422-6.00004-6

Chen, R. R., Silva, E. A., Yuen, W. W., & Mooney, D. J. (2007). Spatio-temporal VEGF and PDGF delivery patterns blood vessel formation and maturation. *Pharmaceutical Research*, *24*(2), 258–264. https://doi.org/10.1007/S11095-006-9173-4/FIGURES/5

Choe, G., Lee, M., Oh, S., Seok, J. M., Kim, J., Im, S., Park, S. A., & Lee, J. Y. (2022). Three-dimensional bioprinting of mesenchymal stem cells using an osteoinductive bioink containing alginate and BMP-2-loaded PLGA nanoparticles for bone tissue engineering. *Biomaterials Advances*, *136*, 212789. https://doi.org/10.1016/J.BIOADV.2022.212789

Coester, C. J., Langer, K., Von Briesen, H., & Kreuter, J. (2000). Gelatin nanoparticles by two step desolvation a new preparation method, surface modifications and cell uptake. *Journal of Microencapsulation*, *17*(2), 187–193. https://doi.org/10.1080/026520400288427

De Witte, T. M., Fratila-Apachitei, L. E., Zadpoor, A. A., & Peppas, N. A. (2018). Bone tissue engineering via growth factor delivery: from scaffolds to complex matrices. *Regenerative Biomaterials*, *5*(4), 197–211. https://doi.org/10.1093/RB/RBY013

Dhakal, S. P., & He, J. (2020). Microencapsulation of vitamins in food applications to prevent losses in processing and storage: A review. *Food Research International*, *137*. https://doi.org/10.1016/J.FOODRES.2020.109326

Donnaloja, F., Jacchetti, E., Soncini, M., & Raimondi, M. T. (2020a). Natural and Synthetic Polymers for Bone Scaffolds Optimization. *Polymers*, *12*(4). https://doi.org/10.3390/POLYM12040905

Donnaloja, F., Jacchetti, E., Soncini, M., & Raimondi, M. T. (2020b). Natural and Synthetic Polymers for Bone Scaffolds Optimization. *Polymers 2020, Vol. 12, Page 905*, *12*(4), 905. https://doi.org/10.3390/POLYM12040905

Feng, X. (2009). Chemical and Biochemical Basis of Cell-Bone Matrix Interaction in Health and Disease. *Current Chemical Biology*, *3*(2), 189. https://doi.org/10.2174/187231309788166398

Ghassemi, T., Shahroodi, A., Ebrahimzadeh, M. H., Mousavian, A., Movaffagh, J., & Moradi, A. (2018). Current Concepts in Scaffolding for Bone Tissue Engineering. *Archives of Bone and Joint Surgery*, *6*(2), 90. https://doi.org/10.22038/abjs.2018.26340.1713

Hollister, S. J. (2009). Scaffold Design and Manufacturing: From Concept to Clinic. *Advanced Materials*, *21*(32–33), 3330–3342. https://doi.org/10.1002/ADMA.200802977

Kahrs, C., & Schwellenbach, J. (2020). Membrane formation via non-solvent induced phase separation using sustainable solvents: A comparative study. *Polymer*, *186*, 122071. https://doi.org/10.1016/J.POLYMER.2019.122071

Kim, J. W., Shin, K. H., Koh, Y. H., Hah, M. J., Moon, J., & Kim, H. E. (2017a). Production of Poly(ε-Caprolactone)/Hydroxyapatite Composite Scaffolds with a Tailored Macro/Micro-Porous Structure, High Mechanical Properties, and Excellent Bioactivity. *Materials 2017, Vol. 10, Page 1123*, *10*(10), 1123. https://doi.org/10.3390/MA10101123

Kim, J. W., Shin, K. H., Koh, Y. H., Hah, M. J., Moon, J., & Kim, H. E. (2017b). Production of Poly(ε-Caprolactone)/Hydroxyapatite Composite Scaffolds with a Tailored Macro/Micro-Porous Structure, High Mechanical Properties, and Excellent Bioactivity. *Materials*, *10*(10). https://doi.org/10.3390/MA10101123

Kim, T., See, C. W., Li, X., & Zhu, D. (2020). Orthopedic implants and devices for bone fractures and defects: Past, present and perspective. *Engineered Regeneration*, *1*, 6–18. https://doi.org/10.1016/J.ENGREG.2020.05.003

Koons, G. L., Diba, M., & Mikos, A. G. (2020a). Materials design for bone-tissue engineering. *Nature Reviews Materials 2020 5:8*, *5*(8), 584–603. https://doi.org/10.1038/s41578-020-0204-2

Koons, G. L., Diba, M., & Mikos, A. G. (2020b). Materials design for bone-tissue engineering. *Nature Reviews Materials 2020 5:8*, *5*(8), 584–603. https://doi.org/10.1038/s41578-020-0204-2

Kozehkonan, G. S., Salehi, M., Farzamfar, S., Ghanbari, H., Adabi, M., & Amani, A. (2019). Preparation and characterization of PCL polymeric scaffolds coated with chitosan/ bioactive glass/gelatin nanoparticles using the tips methodology for bone

tissue engineering. *Nanomedicine Journal*, *6*(4), 311–320. https://doi.org/10.22038/NMJ.2019.06.000009

Li, Y., Ceylan, M., Shrestha, B., Wang, H., Lu, Q. R., Asmatulu, R., & Yao, L. (2014). Nanofibers support oligodendrocyte precursor cell growth and function as a neuron-free model for myelination study. *Biomacromolecules*, *15*(1), 319–326. https://doi.org/10.1021/BM401558C/ASSET/IMAGES/LARGE/BM-2013-01558C_0008.JPEG

Li, Y., Feng, Z., Hao, L., Huang, L., Xin, C., Wang, Y., Bilotti, E., Essa, K., Zhang, H., Li, Z., Yan, F., & Peijs, T. (2020). A Review on Functionally Graded Materials and Structures via Additive Manufacturing: From Multi-Scale Design to Versatile Functional Properties. *Advanced Materials Technologies*, *5*(6), 1900981. https://doi.org/10.1002/ADMT.201900981

Łos, M. J., Skubis, A., & Ghavami, S. (2019). Stem Cells. *Stem Cells and Biomaterials for Regenerative Medicine*, 5–16. https://doi.org/10.1016/B978-0-12-812258-7.00002-2

Loya, K. (2014). Stem Cells. *Handbook of Pharmacogenomics and Stratified Medicine*, 207–231. https://doi.org/10.1016/B978-0-12-386882-4.00011-6

Lukin, I., Erezuma, I., Maeso, L., Zarate, J., Desimone, M. F., Al-Tel, T. H., Dolatshahi-Pirouz, A., & Orive, G. (2022). Progress in Gelatin as Biomaterial for Tissue Engineering. *Pharmaceutics*, *2022*, 1177. https://doi.org/10.3390/pharmaceutics14061177

Maia, F. R., Bastos, A. R., Oliveira, J. M., Correlo, V. M., & Reis, R. L. (2022a). Recent approaches towards bone tissue engineering. *Bone*, *154*, 116256. https://doi.org/10.1016/J.BONE.2021.116256

Maia, F. R., Bastos, A. R., Oliveira, J. M., Correlo, V. M., & Reis, R. L. (2022b). Recent approaches towards bone tissue engineering. *Bone*, *154*, 116256. https://doi.org/10.1016/J.BONE.2021.116256

Milano, F., Masi, A., Madaghiele, M., Sannino, A., Salvatore, L., & Gallo, N. (2023). Current Trends in Gelatin-Based Drug Delivery Systems. *Pharmaceutics 2023, Vol. 15, Page 1499*, *15*(5), 1499. https://doi.org/10.3390/PHARMACEUTICS15051499

Naderi, H., Matin, M. M., & Bahrami, A. R. (2011). Review paper: Critical Issues in Tissue Engineering: Biomaterials, Cell Sources, Angiogenesis, and Drug Delivery Systems. *Http://Dx.Doi.Org/10.1177/0885328211408946*, *26*(4), 383–417. https://doi.org/10.1177/0885328211408946

Neumann, A., Christel, A., Kasper, C., & Behrens, P. (2013). BMP2-loaded nanoporous silica nanoparticles promote osteogenic differentiation of human mesenchymal stem cells. *RSC Advances*, *3*(46), 24222–24230. https://doi.org/10.1039/C3RA44734K

Ntege, E. H., Sunami, H., & Shimizu, Y. (2020). Advances in regenerative therapy: A review of the literature and future directions. *Regenerative Therapy*, *14*, 136–153. https://doi.org/10.1016/J.RETH.2020.01.004

Oliveira, É. R., Nie, L., Podstawczyk, D., Allahbakhsh, A., Ratnayake, J., Brasil, D. L., & Shavandi, A. (2021). Advances in Growth Factor Delivery for Bone Tissue Engineering. *International Journal of Molecular Sciences 2021, Vol. 22, Page 903*, *22*(2), 903. https://doi.org/10.3390/IJMS22020903

Pattnaik, A., Sanket, A. S., Pradhan, S., Sahoo, R., Das, S., Pany, S., Douglas, T. E. L., Dandela, R., Liu, Q., Rajadas, J., Pati, S., De Smedt, S. C., Braeckmans, K., & Samal, S. K. (2023). Designing of gradient scaffolds and their applications in tissue regeneration. *Biomaterials*, *296*, 122078. https://doi.org/10.1016/J.BIOMATERIALS.2023.122078

Pei, B., Hu, M., Wu, X., Lu, D., Zhang, S., Zhang, L., & Wu, S. (2023). Investigations into the effects of scaffold microstructure on slow-release system with bioactive factors for bone repair. *Frontiers in Bioengineering and Biotechnology*, *11*, 1230682. https://doi.org/10.3389/FBIOE.2023.1230682/BIBTEX

Pina, S., Ribeiro, V. P., Marques, C. F., Maia, F. R., Silva, T. H., Reis, R. L., & Oliveira, J. M. (2019). Scaffolding Strategies for Tissue Engineering and Regenerative Medicine Applications. *Materials 2019, Vol. 12, Page 1824*, *12*(11), 1824. https://doi.org/10.3390/MA12111824

Poldervaart, M. T., Wang, H., Van Der Stok, J., Weinans, H., Leeuwenburgh, S. C. G., Oner, F. C., Dhert, W. J. A., & Alblas, J. (2013). Sustained release of BMP-2 in bioprinted alginate for osteogenicity in mice and rats. *PloS One*, *8*(8). https://doi.org/10.1371/JOURNAL.PONE.0072610

Qu, H., Fu, H., Han, Z., & Sun, Y. (2019). Biomaterials for bone tissue engineering scaffolds: a review. *RSC Advances*, *9*(45), 26252. https://doi.org/10.1039/C9RA05214C

Qu, M., Jiang, X., Zhou, X., Wang, C., Wu, Q., Ren, L., Zhu, J., Zhu, S., Tebon, P., Sun, W., & Khademhosseini, A. (2020). Stimuli-Responsive Delivery of Growth Factors for Tissue Engineering. *Advanced Healthcare Materials*, *9*(7), 1901714. https://doi.org/10.1002/ADHM.201901714

Rao, Y. S., & Kamala Kumari, P. V. (2020). Biodegradable nanospheres-current status. *Indian Drugs*, *57*(5), 7–18. https://doi.org/10.53879/ID.57.05.11657

Reddy, M. S. B., Ponnamma, D., Choudhary, R., & Sadasivuni, K. K. (2021). A Comparative Review of Natural and Synthetic Biopolymer Composite Scaffolds. *Polymers 2021, Vol. 13, Page 1105*, *13*(7), 1105. https://doi.org/10.3390/POLYM13071105

Roberts, T. T., & Rosenbaum, A. J. (2012). Bone grafts, bone substitutes and orthobiologics: The bridge between basic science and clinical advancements in fracture healing. *Organogenesis*, *8*(4), 114. https://doi.org/10.4161/ORG.23306

Schrade, S., Ritschl, L., Süss, R., Schilling, P., & Seidenstuecker, M. (2022). Gelatin Nanoparticles for Targeted Dual Drug Release out of Alginate-di-Aldehyde-Gelatin Gels. *Gels*, *8*(6), 365. https://doi.org/10.3390/GELS8060365/S1

Seok, J. M., Rajangam, T., Jeong, J. E., Cheong, S., Joo, S. M., Oh, S. J., Shin, H., Kim, S. H., & Park, S. A. (2020). Fabrication of 3D plotted scaffold with microporous strands for bone tissue engineering. *Journal of Materials Chemistry B*, *8*(5), 951–960. https://doi.org/10.1039/C9TB02360G

Shahrezaee, M., Salehi, M., Keshtkari, S., Oryan, A., Kamali, A., & Shekarchi, B. (2018). In vitro and in vivo investigation of PLA/PCL scaffold coated with metformin-loaded gelatin nanocarriers in regeneration of critical-sized bone defects. *Nanomedicine: Nanotechnology, Biology and Medicine*, *14*(7), 2061–2073. https://doi.org/10.1016/J.NANO.2018.06.007

Subbiah, R., & Guldberg, R. E. (2019). Materials Science and Design Principles of Growth Factor Delivery Systems in Tissue Engineering and Regenerative Medicine. *Advanced Healthcare Materials*, *8*(1), 1801000. https://doi.org/10.1002/ADHM.201801000

Szwed-Georgiou, A., Płociński, P., Kupikowska-Stobba, B., Urbaniak, M. M., Rusek-Wala, P., Szustakiewicz, K., Piszko, P., Krupa, A., Biernat, M., Gazińska, M., Kasprzak, M., Nawrotek, K., Mira, N. P., & Rudnicka, K. (2023). Bioactive Materials for Bone Regeneration: Biomolecules and Delivery Systems. *ACS Biomaterials Science and Engineering*, *9*(9), 5222–5254.

https://doi.org/10.1021/ACSBIOMATERIALS.3C00609/ASSET/IMAGES/LARGE/AB3C00609_0003.JPEG

Tang, D., Tare, R. S., Yang, L. Y., Williams, D. F., Ou, K. L., & Oreffo, R. O. C. (2016). Biofabrication of bone tissue: approaches, challenges and translation for bone regeneration. *Biomaterials*, *83*, 363–382. https://doi.org/10.1016/J.BIOMATERIALS.2016.01.024

Tarhini, M., Greige-Gerges, H., & Elaissari, A. (2017). Protein-based nanoparticles: From preparation to encapsulation of active molecules. *International Journal of Pharmaceutics*, *522*(1–2), 172–197. https://doi.org/10.1016/J.IJPHARM.2017.01.067

Tayalia, P., & Mooney, D. J. (2009). Controlled growth factor delivery for tissue engineering. *Advanced Materials*, *21*(32–33), 3269–3285. https://doi.org/10.1002/ADMA.200900241

Vesvoranan, O., Anup, A., & Hixon, K. R. (2022). Current Concepts and Methods in Tissue Interface Scaffold Fabrication. *Biomimetics*, *7*(4). https://doi.org/10.3390/BIOMIMETICS7040151

Vo, T. N., Kasper, F. K., & Mikos, A. G. (2012). Strategies for controlled delivery of growth factors and cells for bone regeneration. *Advanced Drug Delivery Reviews*, *64*(12), 1292–1309. https://doi.org/10.1016/J.ADDR.2012.01.016

Wang, H., Boerman, O. C., Sariibrahimoglu, K., Li, Y., Jansen, J. A., & Leeuwenburgh, S. C. G. (2012). Comparison of micro- vs. nanostructured colloidal gelatin gels for sustained delivery of osteogenic proteins: Bone morphogenetic protein-2 and alkaline phosphatase. *Biomaterials*, *33*(33), 8695–8703. https://doi.org/10.1016/J.BIOMATERIALS.2012.08.024

Wang, X., Xu, S., Zhou, S., Xu, W., Leary, M., Choong, P., Qian, M., Brandt, M., & Xie, Y. M. (2016). Topological design and additive manufacturing of porous metals for bone scaffolds and orthopaedic implants: A review. *Biomaterials*, *83*, 127–141. https://doi.org/10.1016/J.BIOMATERIALS.2016.01.012

Xia, P., Wang, S., Qi, Z., Zhang, W., & Sun, Y. (2019). BMP-2-releasing gelatin microspheres/PLGA scaffolds for bone repairment of X-ray-radiated rabbit radius defects. *Artificial Cells, Nanomedicine, and Biotechnology*, *47*(1), 1662–1673. https://doi.org/10.1080/21691401.2019.1594852

Xie, G., Sun, J., Zhong, G., Liu, C., & Wei, J. (2010). Hydroxyapatite nanoparticles as a controlled-release carrier of BMP-2: Absorption and release kinetics in vitro. *Journal of Materials Science: Materials in Medicine*, *21*(6), 1875–1880. https://doi.org/10.1007/S10856-010-4038-0/METRICS

Yanar, N., Son, M., Park, H., & Choi, H. (2020). Toward greener membranes with 3D printing technology. *Environmental Engineering Research*, *26*(2). https://doi.org/10.4491/EER.2020.027

Yasmin, R., Shah, M., Khan, S. A., & Ali, R. (2017). Gelatin nanoparticles: A potential candidate for medical applications. *Nanotechnology Reviews*, *6*(2), 191–207. https://doi.org/10.1515/NTREV-2016-0009/ASSET/GRAPHIC/J_NTREV-2016-0009_FIG_005.JPG

Yilgor, P., Tuzlakoglu, K., Reis, R. L., Hasirci, N., & Hasirci, V. (2009). Incorporation of a sequential BMP-2/BMP-7 delivery system into chitosan-based scaffolds for bone tissue engineering. *Biomaterials*, *30*(21), 3551–3559. https://doi.org/10.1016/J.BIOMATERIALS.2009.03.024

Zhang, F., & King, M. W. (2020). Biodegradable Polymers as the Pivotal Player in the Design of Tissue Engineering Scaffolds. *Advanced Healthcare Materials*, *9*(13), 1901358. https://doi.org/10.1002/ADHM.201901358

Zhou, X., Jin, Y., & Du, J. (2020). Functionally Graded Scaffolds with Programmable Pore Size Distribution Based on Triply Periodic Minimal Surface Fabricated by Selective Laser Melting. *Materials 2020, Vol. 13, Page 5046*, *13*(21), 5046. https://doi.org/10.3390/MA13215046